RGD-FUNCTIONALIZED ELECTROSPUN SCAFFOLD FOR ACL TISSUE ENGINEERING

by

Fiona Elizabeth Serack

A thesis submitted to the Graduate Program in Chemical Engineering

in conformity with the requirements for

the degree of Master of Applied Science

Queen's University

Kingston, Ontario, Canada

April, 2017

Abstract

This thesis describes the preparation and evaluation of a biomimetic scaffold for anterior cruciate ligament (ACL) tissue engineering. An electrospun poly(L-lactide-*co*-acrylated trimethylene carbonate) scaffold was functionalized with a peptide containing the arginine-glycine-aspartic acid (RGD) amino acid sequence to increase mechanotransduction and extracellular matrix (ECM) production by fibroblasts seeded on the scaffold surface. The peptide was synthesized by solid phase peptide synthesis and conjugated to the polymer via a Michael-type addition, using a cysteine moiety on the peptide and a maleimide functional group on the polymer. The peptide-polymer conjugate was successfully electrospun with the bulk polymer, resulting in an aligned fibre mat that was crimped and crosslinked to mimic the architecture of native ACL tissue.

Analysis of scanning electron microscope images demonstrated no difference in fibre diameter or scaffold porosity between scaffolds with and without peptide functionalization. There was also no difference in the Young's modulus and toe region of the scaffolds prepared with the functionalized and non-functionalized polymer. Therefore, the inclusion of the RGD peptide did not affect the biomimetic architecture of the electrospun polymer scaffolds.

Rabbit ACL fibroblasts (ACLFs) were attached to the scaffolds, to an extent that was independent of peptide functionalization. Further, scaffolds were cultured under dynamic uniaxial tension to examine the effect of mechanotransduction on the cells. The scaffolds, with and without RGD-modification, were exposed to 10% strain at 1 Hz for 1 h per day. After 12 days, ACLFs cultured dynamically proliferated to a lesser extent than those cultured statically, but produced greater amounts of the collagen and glycosaminoglycan per cell.

Co-Authorship

This thesis contains the original work of Fiona Serack, completed under the supervision of Dr. Brian Amsden. Chapters 1 and 2 were adapted from work prepared as a book chapter that was submitted to the Springer Handbook of Functional Polymers, with Dr. Brian Amsden as a co-author.

Acknowledgements

I would like to express my extreme gratitude to my supervisor, Dr. Brian Amsden, for the opportunity to work with him on this project. His support, guidance, and sense of humor resulted in a fantastic and valuable experience.

Thank you to the current and past members of the Amsden Lab, who made my time here so memorable. In particular: Drs. Dale Marecak, Fei Chen, Roshni Rainbow, and Julian Chesterman for their support, guidance, and patience while sharing their skills; Stuart Young for all the amazing protocols and breaking the no-new-friends rule; and Amanda Brissenden for the caffeine addiction, the valuable beta in and out of the lab, and the unwavering friendship.

I would like to thank both the Connect! NSERC CREATE program and the NSERC CREATE training program in Bone and Joint Health Technologies for providing me with funding and many opportunities to expand my studies outside of the lab. I am also grateful for the NSERC CGS-M and OGS scholarships that helped fund my research.

Finally, thank you to my amazing family and friends for their love, support, and welcome distractions throughout the duration of my project.

Table of Contents

List of Figures

List of Tables

List of Abbreviations

^{1}H NMR	Proton nuclear magnetic resonance
AC	Acryloyl carbonate
ACL	Anterior cruciate ligament
ACLF	Anterior cruciate ligament fibroblast
ASC	Adipose-derived stem/stromal cell
BMSC	Bone marrow-derived mesenchymal stem cell
DCM	Dichloromethane
DMEM	Dulbecco's Modified Eagle Medium
DMF	Dimethylformamide
DMMB	Dimethylmethylene blue
DMSO	Dimethyl sulfoxide
DSC	Dynamic scanning calorimetry
DNA	Deoxyribonucleic acid
dsDNA	Double-stranded deoxyribonucleic acid
ECM	Extracellular matrix
EtOH	Ethanol
FBS	Fetal bovine serum
GAG	Glycosaminoglycan
GRGDS	Glycine-arginine-glycine-aspartic acid-serine amino acid sequence
HBSS	Hank's Balanced Salt Solution
HCl	Hydrochloric acid
HPLC	High performance liquid chromatography
I2959	Irgacure 2959
IKVAV	Isoleucine-lysine-valine-alanine-valine amino acid sequence
MAL	Maleimide
MALDI-TOF	Matrix-assisted laser desorption/ionization - time of flight
MCL	Medial collateral ligament
MSC	Mesenchymal stem cell

OHP	Hydroxyproline
P(LLA-AC)	Poly(L-lactide-co-acryloyl carbonate)
PBS	Phosphate buffered saline
PCL	Poly(ε-caprolactone)
PDLL	Poly(D,L-lactide)
PEG	Poly(ethylene glycol)
PEGDA	Poly(ethylene glycol diacrylate)
PG	Poly(glycolide)
PL	Poly(lactide)
PLCL	Poly(lactide-co-ε-caprolactone)
PLG	Poly(lactide-co-glycolide)
PLL	Poly(L-lactide)
PLLG	Poly(L-lactide-co-glycolide)
RGD	Arginine-glycine-aspartic acid amino acid sequence
SEM	Scanning electron microscopy
TCEP	Tris(2-carboxyethyl)phosphine
TCPS	Tissue culture polystyrene
TE	Tris-EDTA
TEA	Triethylamine
TFA	Trifluoroacetic acid
THF	Tetrahydrofuran
UV	Ultraviolet
WST	Water-soluble tetrazolium salts

Chapter 1

Introduction

The knee is passively stabilized by four ligaments: the lateral collateral, the medial collateral, the anterior cruciate, and the posterior cruciate (Figure 1). The anterior cruciate ligament (ACL) plays an important role in the stabilization of the knee joint, preventing excessive anterior translation and medial rotation of the tibia.[1]

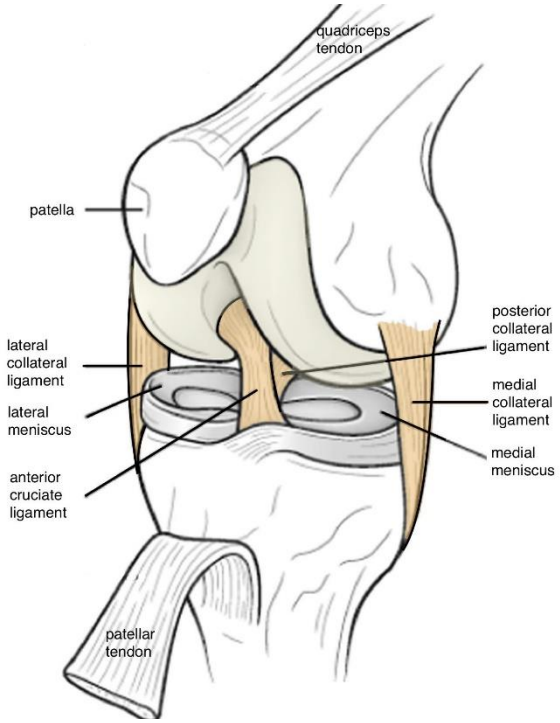

Figure 1: Anatomy of the knee.

1.1 ACL injuries

The ACL is the most frequently injured ligament of the knee, with an estimated annual incidence of 1 per 1000 Americans.[2] ACL tears are common in athletes, with the highest incidences seen in adolescents playing pivoting sports such as soccer, basketball,

volleyball, and skiing; additionally, the incidence rate is 3-5 times higher in women than men.[3–7] Many studies have been done to try and understand the mechanisms involved in ACL injuries, as well as the effects of intrinsic and extrinsic risk factors.[3–7] Several studies have shown that non-contact injuries occur in greater frequency than contact injuries, with non-contact injuries accounting for around 70% of total ACL injuries.[6] Of these non-contact ACL injuries, most occur with the knee approaching full extension, usually in combination with valgus collapse or tibial rotation.[6] While partial tears of the ACL can occur, full ruptures are more common.[8,9]

Unlike the other ligaments of the knee, which are capable of self-repair, the ACL does not heal effectively when injury occurs. This lack of healing is believed to be due to the inability of a blood clot to form around the damaged tissue.[2,10,11] The ACL resides completely within the synovial capsule of the knee and is bathed in synovial fluid which prevents clot formation. Without a clot to form a provisional matrix and stabilize the torn ends of the ACL, cells cannot regenerate the damaged tissue.[2] As a result, the afflicted knee joint cannot properly support daily physiological loads and if left untreated, chondral and meniscal injury occurs and early osteoarthritis sets in.[12] Suture repair of the ACL has been ineffective, with greater than 90% of the patients treated in that manner failing to heal.[13,14] While non-surgical treatment is an option, a study of treatments for ACL injuries showed that early ACL repair and reconstruction can reduce the risk of secondary meniscus tears, and overall is advantageous for the long-term outcome.[15] Surgical reconstruction of the ACL is therefore often required, with an accompanying healthcare cost. Between

100,000-200,000 North Americans annually undergo reconstructive surgery of the ACL, with an associated cost greater than five billion dollars.[16]

1.2 ACL reconstruction surgery

Conventional reconstruction techniques involve the removal of the damaged ACL tissue, and replacement with a tissue capable of withstanding similar loads. Current approaches mainly consist of autografts using the patellar tendon, the hamstring tendon, or the quadriceps tendon.[17] When the patellar tendon is used, portions of the bone are also excised (bone-patellar tendon-bone grafts) to act as insertion sites. Similarly, a quadriceps tendon graft consists of all layers of the tendon, excised with a section of the patella to use as a bone plug.[18] With the hamstring tendon approach, approximately 25 cm is removed from each of the gracilis and semitendinosus tendons, and the tendon segments are folded together to form a strand of quadruple thickness for the replacement graft. Regardless of the graft source, it is typically fixed in place by passing the tissue through holes drilled in the tibia and femur and using suspensory or interference fixation. All three options feature advantages and disadvantages that must be discussed between patient and surgeon. The bone-patellar tendon-bone allows for bone-to-bone healing, which can theoretically result in faster healing, though this method is associated with greater donor site morbidity. The hamstring approach minimizes donor site morbidity and the associated anterior knee pain, but is recommended for patients that are less active.[17] The quadriceps tendon is less studied as a graft, but is considered comparable to the bone-patellar tendon-bone method with respect to its strengths and weaknesses.[19] Although generally successful, conversion of the tendon autograft to ligamentous tissue is a long process (several months), and has the disadvantages of anterior knee pain, decreased range of motion, donor site morbidity, and

limited donor tendon availability.[12,20] Allografts circumvent the disadvantages of donor site morbidity and the need for a secondary surgery, but, could potentially transmit disease, elicit an immunological response, and lose mechanical strength when sterilized, which may result in a failure to integrate with the host tissue.[12,20]

In the early 1970s, orthopaedic surgeons looked for an artificial substitute to mitigate the risks of surgically transmitted infections from allografts, and donor site morbidity related with autografts.[21,22] Biomedical companies responded with ACL prostheses made of polymers including polyester, polypropylene, ultra-high molecular weight polyethylene, polyacrylamide, and polytetrafluoroethylene.[23] These implants had disappointing results, with success rates ranging from 30 – 60%, and many associated problems. A retrospective analysis of various implants demonstrated that the prostheses suffered from abrasion of the textile fibres, and that healing inside the synthetic grafts was poorly organized, incomplete, and unpredictable.[23] Limitations with these surgical approaches have led to the exploration of tissue-engineered ligament grafts to replace conventional techniques.

1.3 Tissue engineering

Tissue engineering combines principles and techniques from the life sciences and engineering to repair or replace damaged and diseased tissues.[24] The development of biomaterials to support tissue repair or growth is an important and significant factor in tissue engineering. Fundamentals within material design, biological signaling, and bioreactors are combined to create a biomimetic template that promotes tissue repair and/or development similar to healthy tissue.

In a recent survey of British orthopaedic surgeons, 86% of the respondents indicated that they would consider using a tissue engineered ACL, if it was biologically and mechanically successful, significantly improved patient outcomes, or shortened surgical time.[25] Moreover, 76% of the respondents indicated that the engineered ACL would be a better choice than the presently used autograft tissues. Thus, there is clearly a strong clinical incentive to create a suitable tissue engineered ACL. The criteria for an engineered tissue are outlined in the following chapter.

Chapter 2

Literature Review

With the design of an engineered ACL, the focus is on material choice and processing methods, scaffold design, cell source, and finally bioreactor conditions. To produce an engineered ACL, replacement tissue is grown in a bioreactor for subsequent implantation in a patient. A scaffold is used to support the seeding of appropriate cells, and this construct is cultured in a cell-supportive environment that provides the appropriate nutrition and regulatory stimuli such as mechanical forces and growth factors. This approach ideally results in a biomimetic tissue capable of withstanding physiological loads within the knee. An engineered construct must simultaneously meet design criteria under all these considerations to be clinically successful.

2.1 ACL structure and function

Three distinct tissue regions can be delineated within the ACL: bone, fibrocartilage, and ligament. The bone region is the point of attachment for the ACL at the femoral and tibial condyles; it is mineralized and inserts into the bone via fibres known as Sharpey fibres. The transition from the stiff bone region to the compliant ligament region is mediated by the fibrocartilage region, which is subdivided into two zones: non-mineralized and mineralized. The non-mineralized zone is characterized by the presence of chondroblasts and ovoid fibroblasts and has a high proteoglycan content, while the mineralized zone consists of hypertrophic fibro-chondrocytes.[26,27] The ligament region contains a sparse population of fibroblasts whose function is to maintain the extracellular matrix (ECM). The fibroblasts are spindle-shaped and make up nearly 20% of the tissue volume. The ECM is

composed 70% w/w water, and the major organic component is collagen (~ 75% dry weight), with < 1% (dry weight) elastin, while proteoglycans (e.g. decorin, biglycan), glycoproteins (e.g. tenascin C), and other cells constitute the rest.[28] The principal collagens in the ligament region are types I and III, in a ratio of approximately 9:1, respectively, while tenascin C is present at a collagen I:tenascin C ratio of 15.7:1.[29]

The collagen molecules are arranged in a hierarchical structure (Figure 2), sequentially assembled into microfibrils, subfibrils, and fibrils (1- 32 μm in diameter). The fibrils are cross-linked to each other, forming fibre bundles called fascicles (100 - 250 μm in diameter) which in turn group together to form the ligament.[28] The fascicles are aligned along the long axis of the ligament and display a wave-like pattern along their length referred to as a crimp. This crimp pattern repeats every 45-60 μm,[28] and plays an important biomechanical role at both the cellular and tissue level.[16]

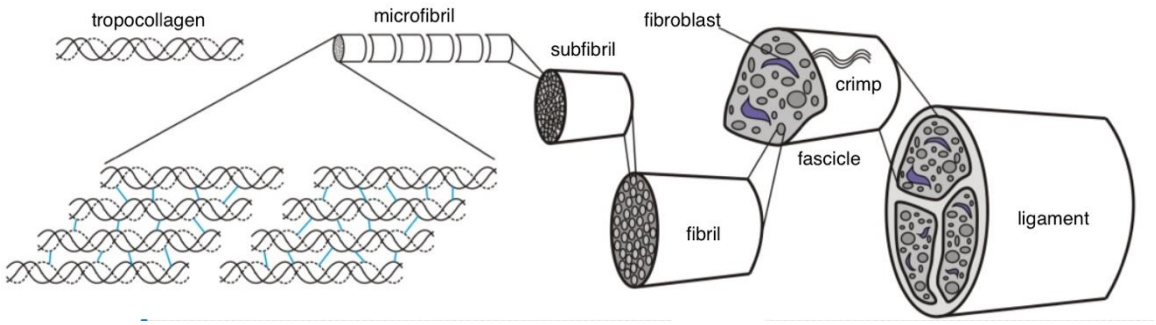

Figure 2: Schematic representation of the structural hierarchy of ligament.

In a healthy individual, the ACL is subjected to dynamic cyclic tensile loads varying from 67 N to 620 N about 1-2 million times per year, depending on the individual's degree of

activity.[30] The ACL exhibits a characteristic triphasic stress-strain response during uniaxial tension (Figure 3). At lower stresses, the unfolding of the crimped fibres yields a non-linear "toe region", between zero strain and 2-5% strain.[31,32] Larger loads transition to the linear stress-strain region, where fibres elongate elastically and the tissue stiffens. As the stress increases further, plastic deformation of the collagen fibres and ligament damage occur, eventually resulting in failure of the bone-ligament-bone complex.[16,33,34] Typical loads applied to the ACL during daily activities exist within the toe and linear regions.[34] The accepted standard mechanical properties of the human ACL are a Young's modulus of 111 ± 26 MPa,[35,36] an ultimate tensile strength of 38 MPa,[35] and 12.8 N-m for energy absorbed at failure.[32]

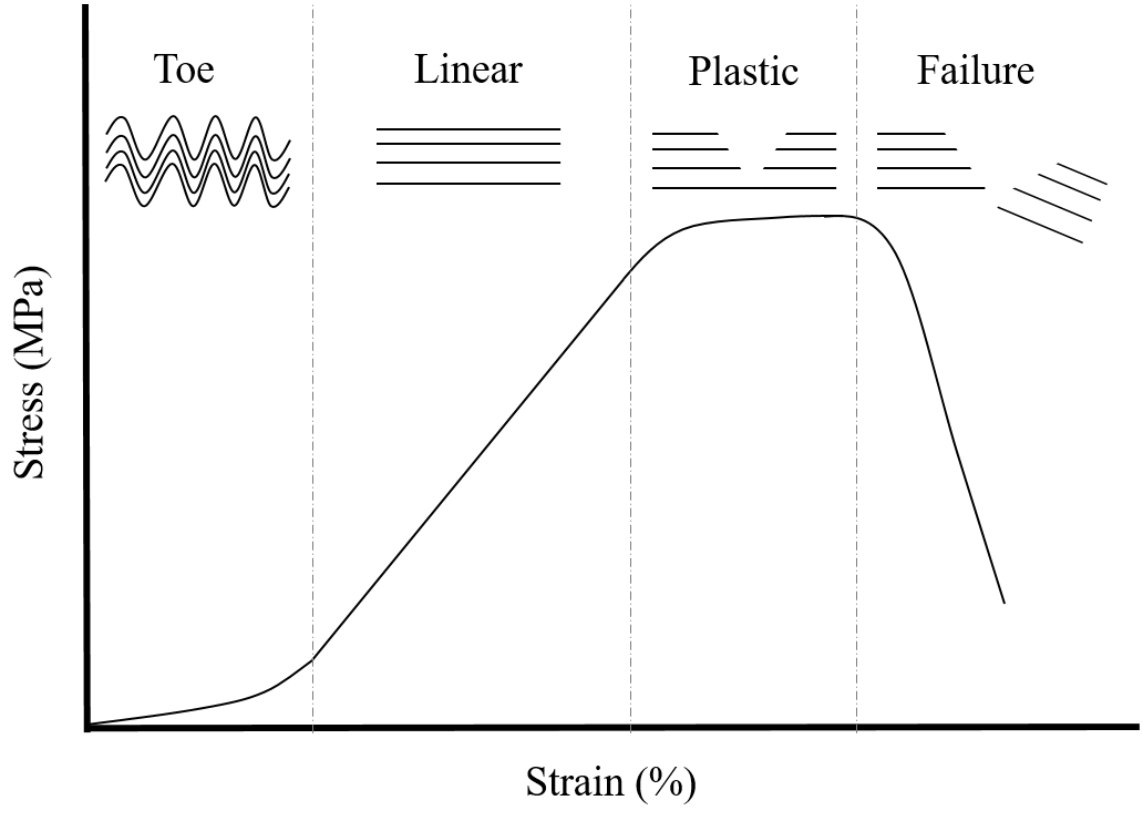

Figure 3: Schematic depicting the triphasic biomechanical behaviour of the ACL. Adapted from Wang, JH. [37]

2.2 Cell Source

An important consideration in tissue engineering and biomaterial design is the cell source, as this will ultimately affect the quality and composition of the developed tissue. The ideal cell source should be easily obtainable and in sufficient quantities, proliferate at an appropriate rate, and generate an ECM similar to that of the native ACL.

2.2.1 Fibroblasts

Fibroblasts are the primary cell type in natural ACL tissue, which makes them an obvious starting point for this application. Fibroblasts from different source tissues are phenotypically different and express different levels and types of collagens.[33] Moreover, ACL fibroblasts (ACLFs) within different regions of the ligament are phenotypically different.[38] The use of ACLFs would be ideal, but, they are available in limited quantity and adult ACLFs grow slowly.[39] Nevertheless, a comparison of fibroblasts isolated from the ACL, the medial collateral ligament (MCL), and the Achilles tendon of rabbits demonstrated that, while MCL and Achilles tendon fibroblasts proliferated faster, the ACLFs had the highest expression of ECM genes specific to the ACL,[40] demonstrating the importance of using ACLFs to generate the appropriate tissue composition.

2.2.2 Stem cells

Adult stem cell sources, and in particular mesenchymal stem cells (MSCs), have been explored as alternatives to ACLFs. MSCs can be isolated from a number of soft connective tissues, such as bone marrow, adipose tissue, the periosteum, peripheral blood, muscle, and the synovium.[41] Of these, the two most intensively studied have been bone marrow-derived MSCs (BMSCs) and adipose-derived stem/stromal cells (ASCs) as they can be readily obtained with minimal potential for long-term tissue damage, they can be expanded rapidly

in vitro, produce ECM quickly, and can be differentiated into a fibroblastic phenotype.[12,42] However, BMSCs must be harvested under general anesthesia and low yields of BMSCs are obtained.[43] In contrast, ASCs can be harvested in a much less invasive procedure and in far greater yields,[44,45] can be cultured *in vitro* for extended periods with stable population doubling, and have a higher proliferation capacity and lower levels of senescence.[46] As such ASCs have been increasingly examined as a potential cell source for ligament tissue engineering.[47]

2.2.3 Co-culture

Nevertheless, neither the use of MSCs nor ACLFs alone have resulted in the generation of an effective replacement ACL tissue. However, recent studies have demonstrated that indirect co-culture of BMSCs with ACLFs increased the expression of collagen I and III and tenascin C by BMSCs, as well as increased their proliferation and total collagen production.[48,49] Moreover, direct co-culture of BMSCs with other cell types such as endothelial cells,[50] tenocytes,[51] and chondrocytes[52] can lead to the effective differentiation of the BMSCs towards the co-cultured cell type. This differentiation is considered to be due to the release of regulatory molecules by each cell type at a sequence determined by interactions between the cells themselves. Recently, Canseco *et al*. reported that direct co-culture of BMSCs with ACLFs on tissue culture polystyrene at a cell ratio of 1:1 resulted in increased expression of the ACL ECM markers collagen I and III and tenascin C,[53] demonstrating the potential of this approach for ACL tissue generation. Furthermore, it has recently been shown that ASCs isolated from porcine patellar fat pads directly co-cultured with ACLFs had significantly increased collagen I gene expression, suggesting differentiation of the ASCs towards a fibroblast phenotype.[54]

2.3 Materials

There are many different biomaterials that can be chosen for tissue engineering applications, but it is important to first consider the criteria for a desirable material. For ACL tissue engineering, the important material characteristics are its mechanical properties, biocompatibility, the biological activity elicited by the material, and its biodegradability. There are several mechanical behaviors and properties that must be met. The most commonly analyzed and compared mechanical properties are the Young's modulus and maximum load at failure. The values for these properties, stated previously, provide standards against which tissue engineered replacements are measured. The material must provide the scaffold with the ability to withstand the dynamic loading conditions the ACL replacement will experience in the body. While there are no "bioinert" materials, the influence of the material and its degradation products on the host tissue response when implanted must be minimal. Ideally, the material would also be cell instructive; it should promote cell attachment, proliferation, induce MSC differentiation if necessary, and ensure appropriate cell morphology and extracellular matrix (ECM) secretion. Many of the scaffolds currently being developed for ACL replacement employ biodegradable polymers. In this regard, the material must degrade in a manner that allows gradual transfer of the applied load from the material to the new tissue being formed as well as cell infiltration into the growing tissue. If material degradation occurs too quickly, the scaffold will not be able to support loading in a bioreactor (*vide infra*) or in the knee following construct implantation. Alternatively, a material that degrades too slowly will not allow for the ingrowth of newly formed tissue.

Many different polymers have been explored as biomaterials for tissue engineered ACL replacements, including natural (e.g. hyaluronan,[55] silk,[56,57] and type I collagen[58–62]) and biodegradable synthetics (e.g. poly(desamino tyrosyl-tyrosine ethyl ester carbonate),[63] poly(L-lactide) (PLL),[40,64] poly(lactide-co-glycolide) (PLG)[39,65]). The different polymers have with their own respective disadvantages and advantages when compared to the design criteria.

2.3.1 Naturally-derived polymers

Type I collagen is the primary structural component of the ACL and is therefore a logical material to examine for ACL tissue generation. Type I collagen-based scaffolds have demonstrated excellent cellular adhesion, with ACL fibroblasts adhering and remaining viable both *in vitro* and *in vivo.*[58,59] However, collagen scaffolds show a reduction in mechanical strength during culture and can be completely resorbed *in vivo.*[66] Collagen scaffolds are therefore crosslinked to increase their mechanical strength, a process that also retards their *in vivo* degradation. A variety of chemical crosslinkers have been used in this strategy, including glutaraldehyde, epoxides, carbodiimides, azides, and nordihydroguaiaretic acid.[67] Many of these options are not considered viable due to issues with cytotoxicity or reversibility of the crosslinks *in vivo.*[68] Physical crosslinking techniques such as UV light or dehydrothermal treatment have also been studied; while they have significantly improved the mechanical properties of the collagen, they tend to have deleterious effects on fibroblast interaction with the fibres.[69,70] Finally, despite the improvement in mechanical properties due to crosslinking, collagen scaffolds have not yet been created that have a modulus equivalent to that of the native ACL.

Naturally-derived polysaccharide-based materials, such as hyaluronic acid, chitosan, and alginate, are frequently used as biomaterials for tissue engineering applications. These materials promote healing, improve cell-biomaterial interactions due to increased protein adsorption, and promote the secretion of growth factors and ECM proteins.[71,72] However, they are generally used in the form of hydrogels and are too weak to use as ligament scaffolds on their own. To take advantage of the biological properties of these materials, several groups have used them as coatings on, or as components of composites with more mechanically robust materials, demonstrating improved cellular attachment and proliferation, and increased ECM synthesis, when compared to non-coated materials.[73–75]

Silk has a history of use as a suture material and so has a demonstrated biocompatibility.[76] Moreover, silk is biodegradable and has mechanical properties matching those of the ACL.[56] Originally there was concern about the cytotoxicity of raw silk from silkworms, due to the allergenic nature of its sericin coating. This issue is mitigated with the use of processed silk, where the coating is removed and the material is considered biocompatible.[77] Silk can be readily modified so as to possess cell recognition sites such as the RGD amino acid sequence to improve cell attachment and proliferation, either chemically[78] or through recombinant techniques.[79] Alternatively, it can be coated with RGD-containing proteins such as collagen or gelatin.[49,80] Silk is a proteolytically degradable material, with a degradation rate dependent on its environment.[76,77] It degrades very slowly, particularly when compared to hydrolytically degradable synthetic polymers.[76] This rate of degradation may be beneficial or problematic, depending on the rate at which neo-tissue formation occurs.

2.3.2 Synthetic polymers

While natural materials possess the important ability to support cell attachment, growth, and differentiation, they are generally enzymatically degraded with kinetics that are not readily predictable or controlled. Further, they are generally weak materials and there is an inherent variability in their properties. Synthetic polymers have the advantage over natural polymers that their properties can be tuned to the desired application. Molecular weights can be readily controlled, and different polymers blended in varying formulations to target mechanical properties and degradation rates. The poly(α-hydroxy esters) such as poly(L-lactide) (PLL), poly(D,L-lactide) (PDLL), poly(glycolide) (PG), poly(lactide-co-glycolide) (PLG), and poly(ε-caprolactone) (PCL) are hydrolytically degradable polymers and have been widely investigated as tissue engineering scaffolds due to their relative ease of synthesis, history of clinical use, and commercial availability.[81] Their hydrolytic degradation is more readily predictable *in vivo* than the degradation of natural materials;[82,83] however, the acidic degradation products have been implicated in a prolonged inflammatory response following implantation.[84] An inherent disadvantage of these materials is their lack of cell recognition sites. However, cell attachment can be improved either through covalent attachment of peptides such as RGD or IKVAV,[85–87] or through coating with proteins such as fibronectin.[88] Another disadvantage of these polymers is that, although they can initially have moduli within the range, or greater than, that of the ACL, they are readily plasticized by the absorption of water, which occurs within 24 h of hydration and causes a notable decrease in modulus.[89] Moreover, they are prone to creep[90] and fatigue failure[91] under dynamic loading. These problems can be addressed by crosslinking the polymer. Crosslinking reduces the rate of water absorption and increases

the glass transition temperature of the polymer, reducing the effect of plasticization, and increasing their resistance to creep and fatigue failure.[90]

2.4 Scaffold Design

With respect to ACL regeneration, tissue engineering strategies have invariably utilized polymer scaffolds. In designing these constructs, it is important to not only consider the nature of the material used, but also the physical structure of the scaffold. A clinically acceptable engineered ACL tissue graft should possess biological architecture and mechanical properties closely aligned with native ACL to allow for physiologic loading after implantation. However, during the remodeling stage of ligament after an injury, the tissue formed is disorganized, hypercellular, and has a significantly different crimp pattern than is present in healthy tissue. As a result of this difference, the healing tissue has reduced mechanical strength, and is vulnerable to re-injury.[92] The optimal generation of replacement ACL tissues would be achieved if the organization of the collagen fibres in the ECM is maintained through the healing process. Therefore, an effective strategy should provide and maintain the necessary mechanical properties to support daily loading, but also needs to facilitate the orientation and alignment of the cells along the direction of applied load. This requirement can be achieved by using a polymer scaffold that has topographical features that regulate the spatial distribution of cell adhesive contacts and the direction of cell spreading. In this context, it is important to produce topographical features at the sub-cellular level (<10 μm).[93–95] Most approaches have focused on the preparation of fibrous polymer scaffolds, which provides control over the scaffold topography.

2.4.1 Knit/ braided scaffolds

In early designs, polymer scaffolds were either knit or braided into "yarns" that could match the mechanical properties of the ACL. For example, Lu *et al*. studied three different compositions of poly(α-hydroxyester) fibres as materials for a braided scaffold: PG, PLL, and 82:18 PLLG.[88] The materials were evaluated with respect to scaffold mechanical properties and degradation, and cell attachment and proliferation. PG was determined to be the strongest scaffold; however, its initial elastic modulus was greater than that of native ACL, and it rapidly lost its mechanical integrity. PLL had an initial elastic modulus most closely resembling native ACL tissue, and a more modest decrease in integrity, indicating that it is a more suitable material for ACL regeneration. The PLL and PLLG scaffolds better supported physiological cell morphology after initial cell attachment than the PG scaffolds. Further, fibres coated with fibronectin prior to cell attachment lead to an increase in cell attachment efficiency and cell proliferation. The fibronectin-coated PLL scaffold supported the highest level of cell proliferation. Based on the results with respect to cell attachment morphology, cell proliferation, and overall mechanical and degradation properties, it was determined that out of the polymer compositions studied, PLL was the most suitable for ACL tissue engineering.

However, the polymer fibres commonly used in braided scaffolds have diameters ranging from 10s to 100s of μm, which are greater than that of the ligament fibroblasts (~10 μm). The use of fibre diameters of this scale result in the cells interacting with a planar surface as opposed to a three-dimensional matrix, like they would in the native tissue. In addition, the use of large fibre diameters and a braided design restricted cell seeding to the outside

of the scaffold, which resulted in poor tissue integration into the scaffolds.[39,40,55,56] While these types of scaffolds supported the mechanical loads of the ACL environment, they lacked the cell-supportive microarchitecture necessary to produce an organized ECM. Chen *et al*.[80] used a scaffold consisting of braided silk fibres with collagen incorporated between the fibres. These scaffolds were seeded with BMSCs, cultured statically for 5 days, and then implanted into a rabbit medial collateral ligament (MCL) model. At 12 weeks, the newly developed tissue was less organized than the native tissue, being significantly weaker and possessing a modulus approximately half of that of native MCL, and had much smaller collagen fibril diameters. Moreover, the MCL model is not indicative of the environment the ACL would experience as the MCL can heal without surgical intervention, while the ACL cannot. In a similar approach, Fan *et al*. employed a knitted silk mesh seeded with BMSCs and wrapped around a braided silk cord.[49] The internal silk cord was necessary to provide the appropriate mechanical properties. BMSCs were seeded onto the scaffold and cultured overnight prior to implantation in a porcine model. After 24 weeks the scaffolds were removed for analysis; the engineered tissue supported roughly half the load of native ACL, and the modulus was less than half that of native tissue. No quantitative assessment of tissue composition was reported, and the tissue did not possess crimped collagen fibres or a toe region when tested in uniaxial tension.

Freeman *et al*. combined two scaffold design techniques, fiber twisting and fiber braiding, to achieve biomimetic mechanical properties with a PLLA scaffold.[96] The braiding angle and twisting angle could be adjusted to alter the ultimate tensile strength of the scaffolds, as well as the length of the toe region. However, some combinations of braid and twist

angles lead to premature scaffold failure. Optimization of the design resulted in a scaffold with a modulus and ultimate tensile strength that exceeded that of the native tissue, and a toe-region of similar length to native ACL. Further, this design was combined with a PEG diacrylate (PEGDA) hydrogel to improve viscoelastic stress dissipation, and was demonstrated to support fibroblast growth *in vitro*.[97] The resulting scaffold had a significantly higher modulus than native ACL tissue, which could cause some difficulties *in vivo* due to stiffness. Further, while fibroblasts demonstrated cellular activity on the scaffolds, proliferation did not increase between days 7 and 28, and no analysis of ECM production and composition was performed.

The introduction of a hydrogel component has been used in several studies to improve the mechanical behaviour of the scaffolds. Dunn *et al.*[98] used extruded collagen fibres (dry diameter 50-70 μm) in a PL solvent-extracted matrix for rabbit ACL reconstruction. Neo-tissue was observed after 4 weeks in 88% of the implanted scaffolds. Also, Gentleman *et al.*[99] used collagen fibres embedded in a cell-seeded collagen hydrogel to create a scaffold to mimic the mechanical and viscoelastic properties of the ACL. Both these scaffold approaches used large fibre diameters to meet the design criteria of ligament-like mechanical properties. Consequently, these scaffolds failed to provide adequate space for *de novo* tissue integration. As a result, the tissue produced was not comparable to native tissue in terms of structure or function.

2.4.2 Electrospinning

Electrospinning has recently been used to develop scaffolds for ACL tissue engineering. Electrospinning is a technique capable of producing polymer fibres on the nanoscale. Such

nanoscale features have the potential to improve cellular interactions and infiltration. In this technique, the polymer is dissolved in an appropriate solvent system, and exposed to a high voltage field resulting in an electronically charged jet of polymer solution eluting from the syringe. The solvent rapidly evaporates, and small fibers are attracted to the collector which is exposed to either an oppositely charged or ground electrode. Different types of collectors can be used to influence the architecture of the fibres. Many parameters in the electrospinning process (concentration, voltage, flow rate, distance from needle to collector, etc.) can be optimized to manipulate the physical properties of the resulting fibrous scaffolds, such as porosity and fibre diameter.[100] This process has been demonstrated to work with many different polymer systems, and is a very promising technique in ACL tissue engineering.

Electrospun fibres have been combined with other scaffold components to improve mechanical properties and biological infiltration. Petrigliano *et al.* developed an electrospun poly(ε-caprolactone) (PCL) scaffold with laser-cut pores to improve vascularization and cell infiltration into the scaffold.[101] While the introduction of pores improved the cellular response and ECM production in the scaffolds, the load to failure and stiffness of PCL are much lower than native tissue, and it is too weak as a homopolymer to support the physiological loads in the ACL.[101] Thayer *et al*. developed a modified electrospinning/spraying technique to produce meshes made of PLG or poly(ester urethane), and included PEGDA hydrogel to reduce the hydrophobicity of the scaffold.[102] As cells were directly electrosprayed into the constructs, cellular infiltration and distribution through the scaffold was improved, but the cells were unable to proliferate and

may therefore not be able to produce adequate ECM. Additionally, the inclusion of the hydrogel phase improved the scaffolds resilience to cyclic loading, but decreased the Young's modulus far below acceptable values for an ACL replacement. Vaquette *et al*. developed a scaffold by combining a knitting technique for high tensile strength and aligned electrospun fibers to improve control over cell seeding.[103] Knit sutures were made from either PLG (10:90 L:G) or silk, and the electrospun fibres surrounding the scaffold were composed of poly(lactide-*co*-ε-caprolactone) (70:30 L:CL). Promisingly, the composite scaffolds had a Young's modulus similar in magnitude to that of native ACL, which is generally not seen in materials made solely of electrospun materials. Additionally, BMSCs attached and proliferated on the scaffolds, while secreting collagenous ECM. Nevertheless, the BMSC study with promising results was only done with the scaffolds made of knitted silk sutures. If shorter degradation times are desired for tissue ingrowth, these tests should be repeated using the PLG knit scaffolds as well.

The Amsden group has recently developed an electrospinning technique that generates nano-/microscale polymer fibres that are uniaxially aligned and that can be induced to crimp along this axis. In this technique, the polymer jet eluted from the needle is collected under tension using a rotating mandrel. Following solvent evaporation, a residual stress remains in the fibres. This stress can be released by either increasing the ambient temperature above that of the glass transition temperature of the polymer, or by reducing the glass transition temperature to below ambient temperature using a plasticizer.[104] Further, the crimp amplitude and frequency can be controlled such that they closely match those of native ligament.[104] This technique can theoretically be applied to

generate aligned, crimped fibres with any polymer that can be electrospun; it has been demonstrated with PLCL,[105] PLL, PDLL, PLG,[89] and a copolymer of lactide and trimethylene carbonate bearing a pendant acrylate group.[90] The crimp pattern has also been shown to be beneficial in generating ACL tissue. Fibroblasts seeded on these scaffolds and cultured under dynamic stretching conditions attached to and aligned along the crimped fibres, proliferated, and synthesized a collagen- and proteoglycan-rich ECM which covered 90% of the fibers by day 14.[105] The ECM composition was consistent with that of native ALC tissue, and fascicle structures formed. This improved response over linear fibres was attributed to generating a maximal cell deformation which triggered appropriate mechanotransduction pathways. Additionally, the Young's modulus of the resulting constructs more than doubled between weeks 2 and 4.[105] Nevertheless, the modulus was only 33 MPa by week 4, which is less than half that of native ACL, suggesting that longer culture times are necessary to produce a suitable tissue for implantation.

2.4.3 Multiphasic scaffolds

Many of the tissue-engineering approaches taken to date have focused on the mid-ligament region of the ACL, with fixation following the approach used with hamstring tendon grafts. Due to the advantages of bone-tendon-bone autografts with respect to faster healing and improved load transfer, some researchers are looking towards multiphasic scaffolds that incorporate the ACL-to-bone interface. Spalazzi *et al.* used poly(lactide-co-glycolide) (PLG) of varying compositions and bioactive glass to prepare a triphasic scaffold with regions to support: A) fibroblast culture and soft tissue formation; B) co-culture of fibroblasts and osteoblasts for fibrocartilage development; and C) osteoblast culture and bone formation.[106] The scaffold was able to support distinct zonal distributions of cells and

phase-specific extracellular matrix deposition over time, demonstrating the feasibility of developing multiple heterogeneous tissues on a single scaffold. Additional studies with the material demonstrated the ability of the scaffold to form and support distinct cellular and matrix regions within a single scaffold, *in vivo.*[107] However, only the compressive modulus of the constructs was investigated, which is an inadequate assessment for the midsubstance region of the ligament. Further, the compressive modulus decreased significantly over time, due to degradation of the material, indicating a potential lack of mechanical stability. He *et al.* used a hybrid silk scaffold and a trilineage co-culture system for *in vitro* bone-ligament interface regeneration.[108] A knitted silk scaffold had a section coated in hydroxyapatite to improve the osteoconductivity, in order to mimic the mineral component of the ECM. Silk scaffolds were seeded with fibroblasts, BMSCs and osteoblasts, cultured separately for 1 week, and then sutured together. BMSCs co-cultured in the region between the fibroblasts and osteoblasts differentiated towards the fibrocartilage lineage, while the fibroblasts and osteoblasts maintained their respective phenotypes. This study demonstrated the potential use of trilineage co-culture to induce a gradual transition region at the ligament-bone interface on polymer scaffolds. Although the group stated that knit silk scaffolds can be produced with appropriate tensile properties, the co-culture technique must be evaluated on uniform, non-sutured scaffolds before it can be used to successfully sustain loads *in vivo*. Ultimately, as more successful scaffolds can be developed for the midsubstance region of the ligament, these techniques can be employed to improve scaffold integration at the bone-ligament interface, ideally resulting in faster healing with better load transfer.

2.5 Bioreactor conditions

Dynamic culture conditions are necessary for effective neo-tissue formation. The health and remodeling of native ligament tissue is dependent on the mechanical forces and/or deformations that are imposed during routine daily activities.[60,109–111] Several ligament tissue engineering studies have demonstrated that cyclic mechanical stretching results in the desired spindle-shaped fibroblast morphology and increased fibroblast proliferation, synthesis of collagen types I and III, and growth factor expression.[112–114]

The ACL is subjected to cyclic, uniaxial stretching during daily activities and this dynamic loading is instrumental to the architecture of the ligament tissue. The highly organized structure of the ACL is maintained by fibroblasts and a number of studies have shown that in response to cyclic stretching, ligament fibroblasts demonstrated enhanced expression of the ligament-associated genes for collagen types I and III,[110,115] as well as tenascin C.[116] The mechanical stretching is transmitted to the fibroblasts through the ECM via cell membrane mechanosensors. These mechanosensors (such as focal adhesion complexes, discoidin domain receptors, stretch-activated ion channels) react in response to mechanical stimulation by activating signaling cascades that produce ECM components, enzymes, or signaling molecules such as growth factors and cytokines.[88,117] This interaction is considered essential for the generation and maintenance of an organized ECM with the appropriate mechanical properties to support physiological loading.

2.5.1 Integrin-binding modifications

As discussed above, the ACL is characterized by a triphasic stress-strain response that is a result of its crimped and aligned collagen fibre microstructure. Therefore, to generate an

effective replacement ACL, it is necessary to create a scaffold possessing the characteristic architecture of native ligament to stimulate the appropriate mechanotransduction pathways. However, many of the scaffold materials examined to date possess few cell recognition sites, and so cell attachment, and thus transmission of mechanical signaling, is poor. Modification of fibre surfaces with proteins,[88,117] polysaccharides,[118,119] or peptide sequences[120] has been used to improve cellular adhesion, proliferation and ECM production in comparison to the unmodified scaffolds. Coating fibres with adhesive proteins or peptide ligands, such as the integrin-binding glycine-arginine-glycine-aspartic acid-serine (GRGDS) sequence, can improve cell attachment; however, as the polymer material that makes up the fibres degrades, these signals are lost. Additionally, competitive binding of proteins and other molecules in the serum can displace these signal molecules from the surface. An approach to overcome these problems would be to incorporate adhesive binding sites directly onto the backbone of the polymer used to create the fibres; in this way, fresh peptide ligands will be exposed as the polymer degrades. Moreover, the mechanical forces generated by stretching the polymer fibres will be directly transmitted to the cells.

Of the peptide ligands derived from the ECM, those recognized by integrins have been the most studied with respect to their mechanotransductive action.[121] However, there is a significant lack of understanding of the role of integrins during ligament healing and in the mechanisms of integrin mechanotransduction. What is known is that the $\alpha 5\beta 1$ integrin is up-regulated in ligament fibroblasts in response to cell injury[114,122] and the expression of this integrin increases significantly when these cells are exposed to dynamic loading in

culture,[109] suggesting that the receptor for this integrin is important for ligament repair. Furthermore, ACLFs isolated from the midsubstance region of the ACL exhibited stretch-activated collagen gene expression levels that were dependent on integrin αvβ3-mediated cellular adhesions.[123] This result suggests that αvβ3-mediated stretch signal transduction might be effective in stimulating collagen gene expression in human ACLFs. Both the α5β1 and αvβ3 integrins bind to the RGD sequence.[124] MSCs also express these integrins,[78] thus, it is reasonable to examine RGD containing peptides as ligands for promoting effective ligament tissue production.

There have been few studies wherein the influence of a peptide binding ligand has been employed to enhance ACLF interactions with a polymer substrate for ligament tissue engineering purposes. Of the studies done to date, all have used an RGD motif. Chen *et al*. grafted the GRGDS peptide onto aligned silk fibres and examined the influence of the GRGDS on human ACLFs and BMSCs under static culture conditions.[78] The presence of GRGDS improved initial ACLF and BMSC seeding efficiency, but did not increase proliferation rates of either cell type. Furthermore, there was not a significant difference in collagen type I production per cell for either cell type after 14 days in the presence or absence of the peptide. In contrast, in a recent study by Wang *et al*., porcine ACLFs seeded onto GRGDS grafted poly(styrene) films possessing nanometer-sized aligned grooves produced significantly more collagen type I per cell after 14 days in static culture.[125] Thus, the influence of RGD on ACL fibroblasts is presently unclear. The difference in the two results may be due to differences in the diameter of the silk fibres (~10-20 μm) versus the grooves (800 nm), the co-culture with MSCs in Chen's study, or may have been a result of

differences in the degree of RGD conjugation. Chen *et al*. report a GRGDS surface density of 7.2 pmol/cm^2,[78] while Wang *et al*. did not quantify the surface density of GRGDS. Additionally, both studies utilized static conditions and as discussed above, cyclic loading during culture results in upregulated integrin expression, and so more effective responses would be expected with dynamic culture conditions.

2.5.2 Cyclic loading

Although it is established that cyclic loading during culture improves tissue formation (in terms of tissue composition and cell morphology and orientation), there have been few long-term studies examining the influence of the loading conditions on the tissue formed. Noth *et al*. reported that 1 Hz, 8h/day stretched to a strain amplitude of 12% and cultured for 14 days, increased collagen I and III gene expression of human MSCs seeded onto collagen scaffolds compared to non-stretched controls,[60] while Kreja *et al*. reported that 1 Hz, 1h/day, stretched to a strain amplitude of 5% and cultured for 15 days upregulated collagen I and III as well as tenascin C gene expression in human ACLFs seeded on poly(lactide) microfibers.[110] A frequency of 1 Hz over a limited time period per day was chosen by these researchers to reflect the physiological loading of the ACL.[105] Surrao *et al*. have shown that bovine fibroblasts seeded onto crimped poly(lactide) fibres and cultured at a strain rate of 10% with a frequency of 1 Hz for 3 h/day over 3 days generated tissue with a collagen to glycosaminoglycan ratio similar to that of native ACL.[105] Moreover, optimal culture conditions with respect to tissue composition and mechanical properties were obtained upon straining the scaffolds beyond the toe region, and into the linear stress-strain region. The fibroblasts formed collagen bundles that resembled fascicles, a characteristic hierarchical feature of ligaments, and the biochemical

composition of the tissue was similar to that of native ACL with respect to the collagen types present (I and III) and the ratio of collagen to sulfated proteoglycans.[105] These findings have recently been confirmed with ligament fibroblasts by Chao *et al*. who have used the same crimping technique.[126]

Chapter 3

Project Scope

As the ACL is a complex tissue, a major difficulty in designing an appropriate polymer scaffold for tissue regeneration is achieving both appropriate mechanical and biological properties. While many studies primarily focus on one aspect or the other, it can be appreciated that both criteria must be considered to develop a functional and clinically relevant engineered replacement. Despite the work done to date, no engineered ACL tissue has the appropriate extracellular architecture or mechanical properties to lead to success following *in vivo* transplantation. This failure is primarily due to two factors: 1) the lack of scaffolds with biomimetic architecture and mechanical properties capable of supporting ligament tissue development *in vitro* and remodeling *in vivo*, and 2) the use of ineffective cell sources; neither MSCs nor ACLFs alone have generated appropriate ACL tissue, *in vitro* or *in vivo*, regardless of the scaffold design. The different criteria and techniques discussed need to be further considered and employed to develop an engineered polymer scaffold that can successfully supersede the current ACL replacement techniques.

1.4 Previous work

The research done in this thesis was the next step in a series of studies by the Amsden group with the goal of producing a biomimetic polymer scaffold for ACL regeneration. It is therefore important to understand the successes and shortcomings of these previous studies.

Hayami *et al*.[75] first focused on the development of an electrospun fibrous scaffold, in an attempt to mimic the aligned collagen fibrils in native ACL tissue. A hydrogel was included to mimic the hydrated portion of the ACL, provide lubrication between fibres, and distribute the cells evenly through the scaffold. Various materials were investigated in the project with the most promising found to be poly(ε-caprolactone-co-D,L-lactide) copolymer fibres, base-etched to improve cellular attachment, with a methacrylated glycol chitosan hydrogel to deliver encapsulated MSCs. Crimp in the fibres was solely due to residual stress loss when removing the fibres from the rotating mandrel.

Surrao *et al*.[104] further investigated the crimping effect using electrospun poly(L-lactide-co-ε-caprolactone) fibres. It was found that the crimping effect was a result of the residual stresses in the fibres and a difference between the operating temperature (T_{op}) and the glass transition temperature (T_g). Ultimately, after removal from the rotating mandrel, the electrospun fibres could be induced to crimp by exposing them to temperatures above the T_g of the material. The crimp parameters could be altered based on the difference between the T_g and T_{op}; with ΔT of 11°C the crimp amplitude and wavelength were 9 ± 0.6 μm and 51 ± 1.8 μm, respectively. These values were comparable to reported values for human ligament of 5 – 10 μm for the crimp amplitude and 45 – 60 μm for the wavelength.[104] These crimped fibres exhibited a toe region in their stress-strain profile that mimicked that of native ACL tissue. Further, the crimp pattern was retained during the *in vitro* degradation of the material, and bovine fibroblasts were shown to attach, proliferate, and produce ECM on the surface of the fibres.

The crimp process was demonstrated with poly(L-lactide-co-D,L-lactide) (PLDLA), poly(D,L-lactide) (PDLLA), poly(L-lactide) (PLLA), and poly(L-lactide-co-glycolide) (PLGA).[89] Of the formulations tested, 250 kDa PLDLA possessed the highest modulus and was the most resistant to *in vitro* degradation, shown over a 6-month period. The crimp pattern appeared to aid the deposition of ECM molecules, as cells and collagen were observed both at the surface and in the interior regions of the scaffold, demonstrating improved cellular infiltration compared to other scaffold designs (e.g. knits/ braids).

Further, the effect of dynamic uniaxial tension during culture conditions was tested on bovine fibroblasts adhered to the scaffolds.[105] Strain amplitudes of 5, 10, and 20% were investigated with both crimped and uncrimped fibres, and compared to static controls. The results demonstrated that dynamic mechanical loading of fibroblasts seeded on crimped fibre scaffolds elicited significant increases in ECM synthesis and accumulation. A strain magnitude of 10% resulted in tissue most similar to that of native ligaments. However, the crimp pattern was shown to not be completely recoverable in the materials upon repetitive loading. Additionally, the hydrated modulus of the scaffolds, both initially and after 8 weeks of culture, was low in comparison to native ACL tissue.

To remedy the issues of low modulus and a lack of stability in the crimp architecture, Chen *et al*. co-polymerized L-lactide with an acryloyl carbonate monomer.[90] This yielded a copolymer with pendant acrylate groups that could be used to crosslink the electrospun fibres after the crimping process. Crosslinking the scaffolds significantly increased the Young's modulus of the samples. Further, while uncrosslinked scaffolds demonstrated an

increase in gauge length over 10 pull-relaxation cycles, crosslinked scaffolds demonstrated only a modest increase between cycles 1-4, followed by a plateau, indicating that the crimp pattern was more recoverable. The crimp pattern was retained during 5 weeks of *in vitro* degradation. While 3T3 fibroblasts were able to attach to and proliferate on the scaffolds, no ECM deposition was quantified.

1.5 Proposed approach

To improve upon the previous designs, the next step was to improve cellular attachment and infiltration. This would ideally improve cell retention to the scaffolds, resulting in greater ECM deposition, and ultimately a greater Young's modulus. While it was important to maintain the biomimetic architecture of the previous scaffolds' design, modification with cell-adhesive peptide ligands was necessary to improve mechanotransduction, and ECM production. Based on the literature, including the RGD binding site had great potential. It was determined that the best approach was to incorporate the peptide sequence directly into the polymer formulation for electrospinning, to ensure that the ligands will continue to be present as the polymer degrades, and so that mechanical stimulation to the fibres will be translated directly to the cells.

The challenge was that the chosen P(LLA-AC) formulation used previously is hydrophobic, while the peptide is hydrophilic. While it was possible to graft the peptide directly to the pendant acrylate groups using a Michael-type conjugate addition, the conjugation changed the solubility of the polymer in the electrospinning solution. This meant that the polymer could not be electrospun (unpublished results). To remedy this, an alternative approach was proposed, involving the introduction of a PEG spacer between

the peptide and the polymer, with the aim of increasing the solubility of the conjugate in organic solvents. With this approach, the addition of a maleimide functional group was also considered; Michael-type addition will preferentially conjugate the cysteine moiety to the maleimide group instead of the acrylate group,[127] preserving its functionality for crosslinking of the polymer.

1.6 Objectives

The goal of this thesis was to develop a scaffold that mimics the biological structure and surface properties of native ACL, and which, when seeded with ACLFs, and cultured under dynamic conditions, generates tissue resembling native ACL in structure and function. The project is further divided into two specific aims:

Specific Aim 1: To develop a biodegradable P(LLA-AC) scaffold possessing a stable crimp pattern and Young's modulus approximating that of native ACL tissue, modified with RGD peptide sites to enhance cell attachment.

Specific Aim 2: To evaluate ACLF proliferation and ECM expression under static and dynamic conditions on the scaffolds prepared in Aim 1.

Chapter 4

Methods and Materials

4.1 Polymer Preparation

4.1.1 Materials

All materials were used as received unless otherwise noted. All materials used in the polymer preparation section, unless otherwise specified, were obtained from ThermoFisher Scientific (MA, USA). Chloroform-d, and 2,2′-(ethylenedioxy)diethanethiol were obtained from Sigma-Aldrich (MO, USA). Hetero-bifunctional PEG with a maleimide functional group and a hydroxyl functional group (HO-PEG-Mal) (2 kDa) was obtained from Laysan Bio, Inc. (AL, USA), Novabiochem Oxyma Pure (ethyl cyano(hydroxyimino)acetate) was obtained from Merck Millipore (MA, USA), 100% ethanol was obtained from Commercial Alcohols (ON, Canada), and tris(2-carboxyethyl)phosphine (TCEP) was obtained from Soltec Ventures (MA, USA). Amino acids (G, C, Y, R, D, S, P), and Fmoc-Gly-Wang resin were obtained from AAPPTec (KY, USA). L-Lactide was obtained from Purac Biomaterials (The Netherlands) and purified by recrystallization in anhydrous toluene. Tetrahydrofuran (THF) was dried with 4 Å molecular sieves for 2 days before use in anhydrous reactions.

4.1.2 Synthesis of acryloyl carbonate (AC)

AC monomer was synthesized according to a 4-step reaction protocol, adapted from Chen, W. *et al*.,[128] and Chen, F. *et al*.,[90] summarized in the schematic shown in Figure 4. Sample structure and purity was confirmed after each step using ^{1}H NMR spectra obtained from a

Bruker Avance-400 MHz spectrometer. All NMR samples were run in chloroform-d, using tetramethylsilane (TMS) as an internal reference for chemical shift calibration.

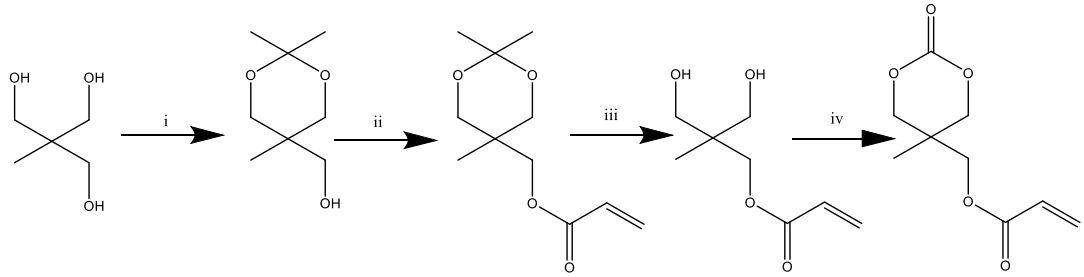

Reaction conditions: (i) 2,2-dimethoxypropane, *p*-toluenesulfonic acid monohydrate, acetone, room temperature; (ii) acryloyl chloride, triethylamine, tetrahydrofuran, 0 °C; (iii) HCl (11.6 M), methanol, 0 °C/ room temperature; (iv) ethyl chloroformate, triethylamine, tetrahydrofuran, 0 °C.

Figure 4: Schematic showing all four steps of AC monomer synthesis. Adapted from Chen et al.[128]

4.1.2.1 Preparation of (2,2,5-trimethyl-1,3-dioxan-5-yl)methanol

Tris(hydroxymethyl)ethane (19.9930 g, 166 mmol) was dissolved in acetone (175 mL) in a 500 mL round bottom flask. To this solution, 2,2-dimethoxypropane (22.4 mL, 182 mmol) was added under constant mixing, followed by *p*-toluenesulfonic acid monohydrate (0.3174 g, 1.669 mmol). The reaction was allowed to proceed for 2 h, then quenched with potassium carbonate (8.01 g, 58.0 mmol). The resulting white precipitate was removed by filtration and washed with diethyl ether. The combined filtrate was concentrated *in vacuo* to yield a colorless oil of (2,2,5-trimethyl-1,3-dioxan-5-yl)methanol (23.4 g, 87.8%). Purity was confirmed by ^{1}H NMR, before use in the next step.

4.1.2.2 Preparation of (2,2,5-trimethyl-1,3-dioxan-5-yl)methyl acrylate

A 250 mL round bottom flask was flame dried and purged with argon, before being charged with (2,2,5-trimethyl-1,3-dioxan-5-yl)methanol (16 g, 0.10 mol) and anhydrous THF

(65 mL). The flask was placed in an ice bath to lower the temperature to 0 °C, followed by slowly injecting triethylamine (32 mL, 0.229 mol), yielding a pale yellow solution. Acryloyl chloride (16.18 mL, 0.20 mol) was slowly added dropwise to the mixture. The temperature was maintained at 0 °C for 30 minutes, after which the vessel was allowed to warm to room temperature overnight, as the reaction continued. The precipitate (TEA·HCl salt) was removed by vacuum filtration, and rinsed several times with THF, until it ran clear. The filtrate was concentrated *in vacuo*, and the purity of the product (yield 21.0 g, 98.0%) was confirmed using ^{1}H NMR.

4.1.2.3 Preparation of 3-hydroxy-2-(hydroxymethyl)-2-methylpropyl acrylate

(2,2,5-trimethyl-1,3-dioxan-5-yl)methyl acrylate (10 g, 46.67 mmol) and methanol (100 mL, 0.5 M) were added to a 250 mL round bottom flask and stirred for 5 min, until the solution turned a uniform, pale yellow. The vessel was placed in an ice bath and cooled to 0 °C before the other reagents were added. Concentrated hydrochloric acid (HCl) (11.6 M) (4.74 mL, 55 mmol) was added dropwise to the flask, after which the reaction was allowed to mix for 4 h as it warmed to room temperature. The vessel was then returned to an ice bath and cooled to 0 °C for neutralization. The aqueous solution was neutralized to a pH of 7 with triethylamine (7.67 mL, 55 mmol), confirmed using pH paper. The aqueous phase was then extracted three times with chloroform. The organic phase was dried over magnesium sulfate, filtered, and concentrated *in vacuo*, with the heat controlled to maintain room temperature. The resulting product was dissolved in minimal THF to precipitate any residual TEA·HCl salts. The salts were removed with filtration, and the filtrate was again concentrated *in vacuo* at room temperature. The purity of the product (yield 6.4 g, 78.4%) was confirmed with ^{1}H NMR.

4.1.2.4 Preparation of Acryloyl carbonate (AC)

A flame-dried round bottom flask was purged with argon and charged with 3-hydroxy-2-(hydroxymethyl)-2-methylpropyl acrylate (4.7 g, 26.98 mmol), ethyl chloroformate (6.4 mL, 67.45 mmol), and anhydrous THF (150 mL). The vessel was cooled to 0 °C in an ice bath with constant mixing. Triethylamine (9.5 mL, 67.4 mmol) was slowly added dropwise, after which the reaction was allowed to proceed for 4 h at 0 °C. The mixture was filtered, and the filtrate was concentrated *in vacuo*. The resulting oil was crystallized from diethyl ether (10 mL) to yield the desired monomer, acryloyl carbonate (yield 2.94 g, 64%). The monomer was further dried using lyophilisation in preparation for polymerization, and stored at -20 °C, protected from light, until needed. Purity was confirmed using ^{1}H NMR.

4.1.3 Synthesis of P(LLA-AC)

The polymerization was carried out in toluene at 110 °C using tin(II) 2-ethylhexanoate ($Sn(Oct)_2$) as a catalyst, and 1-octanol as an initiator, when required. Polymerizations were carried out under different initiator conditions (1:500, 1:1000 and no initiator) to alter the molecular weight of the polymer. The following is an example synthesis, targeting 20 mole% AC in the resulting polymer. An oven-dried glass ampoule was purged with argon, and charged with L-lactide (3.4558 g, 24 mmol), AC (1.2 g, 6.0 mmol) and anhydrous toluene (6 mL). The reaction vessel was purged with argon, after which 1-octanol (7.8 mg in 780 μL toluene) and $Sn(Oct)_2$ (24.3 mg in 1215 μL toluene) were quickly added. The vessel was purged with argon using a long needle into the solution for 5-10 min, then flame-sealed under vacuum and placed in an oil-bath at 110 °C. The reaction was allowed to proceed with constant mixing for 24 h, then the ampoule was removed from the heat and allowed to cool to room temperature. Toluene was removed

under a stream of air, then the sample was dissolved in dichloromethane (DCM) and precipitated in cold (-20 °C) diethyl ether. The resulting polymer was dried in a vacuum desiccator at room temperature. The product was lyophilized and stored at -20 °C, protected from light, until further use.

^{1}H NMR spectra obtained from a Bruker Avance-400 MHz spectrometer was used to confirm the structure and purity of the copolymer and calculate the mole percentage of AC present. Samples were run in chloroform-d, using TMS as an internal reference. The molecular weight of the polymer samples was characterized by gel permeation chromatography (GPC). Samples were dissolved in high performance liquid chromatography (HPLC) grade THF at a 2 mg/mL concentration and filtered with a 0.2 μm syringe filter. The GPC system consisted of a Waters 2690 separation module equipped with four Waters Styragel HR columns in series, and a Waters 410 Differential Refractometer. Refractive index measurements were collected at 25 °C using distilled THF as the eluent, and calibrated to polystyrene standards. The glass transition temperature (T_g) of the polymers was measured using a Mettler Toledo DSC1 system. The samples were taken through two heating cycles and one cooling cycle. The heating cycles ran from −80 to 180 °C, while the cooling cycle ran from 180 to −80 °C. A 10 °C/min heating rate with a 3 min hold time at each set point; T_g was measured from the second heating cycle.

4.1.4 Synthesis of MAL-PEG-P(LLA-AC)

A 5 mL flame-dried ampoule was cooled in a 65 °C oven and purged with argon, then charged with HO-PEG-Mal (2 kDa) as an initiator (199 mg, 0.1 mmol), L-lactide (401 mg, 2.8 mmol), AC (141 mg, 0.7 mmol), and anhydrous toluene (1.1 mL). The vessel was

purged with argon, then $Sn(Oct)_2$ (5 mg in 250 μL toluene) was added. The vessel was purged with argon using a long needle inserted into the solution for 5-10 min, then flame-sealed under vacuum and placed in an oil-bath at 110 °C. The reaction was allowed to proceed with constant mixing for 24 h, then the ampoule was removed from the heat and allowed to cool to room temperature. Toluene was removed under a stream of air, then the sample was dissolved in DCM and precipitated in cold diethyl ether. The resulting polymer was dried in a vacuum desiccator at room temperature, then lyophilized and stored at -20 °C, protected from light, until further use. The product was analyzed using ^1H NMR spectra from a Bruker Avance-400 MHz spectrometer to confirm purity, and to calculate AC fraction and number average molecular weight. Samples were run in chloroform-d, using TMS as an internal reference

4.1.5 Synthesis of GPSDGRGYGCG peptide

4.1.5.1 Solid-phase peptide synthesis

The GRGDS-containing 11-mer peptide was synthesized by solid-phase peptide synthesis on an automated peptide synthesizer (Liberty Blue) using Fmoc-Gly-Wang resin, Fmoc-Gly-OH, Fmoc-Cys(Trt)-OH, Fmoc-Tyr(tBu)-OH, Fmoc-Arg(Pbf)-OH, Fmoc-Asp(OtBu)-OH, Fmoc-Ser(tBu)-OH, and Fmoc-Pro-OH, according to the manufacturer's instructions. The synthesis was performed on a 0.25 mmol scale, using 0.806 g of resin. The deprotection and activation solutions were prepared immediately before use. Deprotection solution was made by dissolving 9 g piperazine and 1.4 g oxyma in 20 mL of a 1:1 mixture of dimethylformamide (DMF) and ethanol, which was then diluted with 80 mL DMF to a ratio of 9:1 DMF:ethanol, and final concentrations of 9 g piperazine/100 mL and 1.4 g oxyma/100 mL. Two activator solutions were prepared for the coupling of

amino acids. The Activator (Act) solution, used to activate the carboxyl terminus for the condensation reaction, was made by mixing 3.9 mL of N,N'-diisopropylcarbodiimide with 46.1 mL of DMF. The Activator B (Act B) solution, used to reduce epimerization of the peptide due to carbodiimide activation of amino acid derivatives, was made by dissolving 3.55 g oxyma in 25 mL DMF. After the synthesis was completed, the resin-bound peptide was transferred from the reaction vessel to a 50 mL conical tube with DCM rinsing, and stored at 4 °C overnight, until resin detachment and purification.

4.1.5.2 Resin detachment

Resin-bound peptide was transferred in DCM to a plastic column cartridge fitted with a glass filter. DCM was allowed to drain through the column, and the resin was rinsed with additional DCM to remove residual DMF from the synthesis process. Air pressure was used to force residual DCM through the column and dry the resin. A solution of Type 1 water (9 drops), 2,2′-(ethylenedioxy)diethanethiol (9 drops), and triisopropylsilane (9 drops) in trifluoroacetic acid (TFA) (5 mL total volume) was added. The column was purged with argon, sealed, and allowed to react for 1-2 h at 37 °C under gentle agitation. The column was uncapped, and the TFA solution was filtered and collected in a 50 mL conical tube. The resin, left in the column, was rinsed with additional TFA (1 mL), similarly collected using air pressure to force residual TFA through the resin beads and filter. The solution was concentrated under a stream of argon, and then precipitated using diethyl ether at -20 °C. The mixture was allowed to precipitate at -20 °C for 4 h, then centrifuged and decanted to remove the ether. The solid mass was dissolved in TFA (1 mL), and the precipitation was repeated with diethyl ether for 72 h at -20 °C. After decanting the second precipitation, the solid pellet was physically broken up, and washed

twice with cold diethyl ether to dilute and remove residual TFA, 2,2′-(ethylenedioxy)diethanethiol, and triisopropylsilane. Residual diethyl ether was evaporated from the solids under argon. A solution of 2% v/v acetic acid in Type 1 water (30 mL) was prepared, and degassed with argon sparging to avoid oxidation of cysteine residues to form disulfides. The dried solids were dissolved in the acetic acid solution, frozen in liquid nitrogen, and lyophilized. Samples were analyzed using matrix-assisted laser desorption/ionization – time of flight (MALDI-TOF) spectrometry by the Protein Function Discovery lab at Queen's University.

4.1.5.3 Peptide purification

High performance liquid chromatography (HPLC) was performed using a Waters HPLC system equipped with a Waters 600 Controller, Waters 717plus Autosampler, Waters 2487 Dual λ Detector measuring UV at 254 nm, and a Synchronis C18 column. Two solvent solutions were prepared: Solvent A, type 1 water + 0.1% TFA and solvent B, 20% type 1 water + 80% HPLC grade acetonitrile + 0.1% TFA. Samples were dissolved in a 50:50 mixture of solvents A and B at 10 mg/mL and filtered through a 0.22 μm filter. The greatest separation was achieved using a 60:40 ratio of solvents A and B, and a flow rate of 5 mL/min, with fractions collected in the peak at 10 min retention time. The collected fractions were dried under a stream of air, dissolved in a 2% v/v acetic acid in type 1 water solution, frozen in liquid nitrogen and lyophilized. Purified samples were again analyzed using MALDI-TOF by the Protein Function Discovery lab at Queen's.

4.1.6 Conjugation of peptide to MAL-PEG-P(LLA-AC)

A 10 mL glass screw-top vial was purged with argon and charged with MAL-PEG-P(LLA-AC) (100 mg, 16.7 mmol), GPSDGRGYGCG peptide (36 mg, 33.5 mmol), and DMF (3.5

mL). The solution was purged with argon using a long needle inserted into the solution, then sealed and allowed to react with constant mixing for 24 h. The DMF was evaporated under a stream of air, and the conjugated product was precipitated using cold diethyl ether. The product was lyophilized and stored at -20 °C, protected from light, until further use. Conjugation was confirmed via ^{1}H NMR using a Bruker Avance-400 MHz spectrometer. Samples were run in both chloroform-d, and a 50:50 mix of deuterated chloroform and dimethyl sulfoxide (DMSO), all using TMS as an internal reference.

4.2 Scaffold fabrication

The processes involved in the preparation of the electrosun polymer fibre scaffolds are depicted in Figure 5.

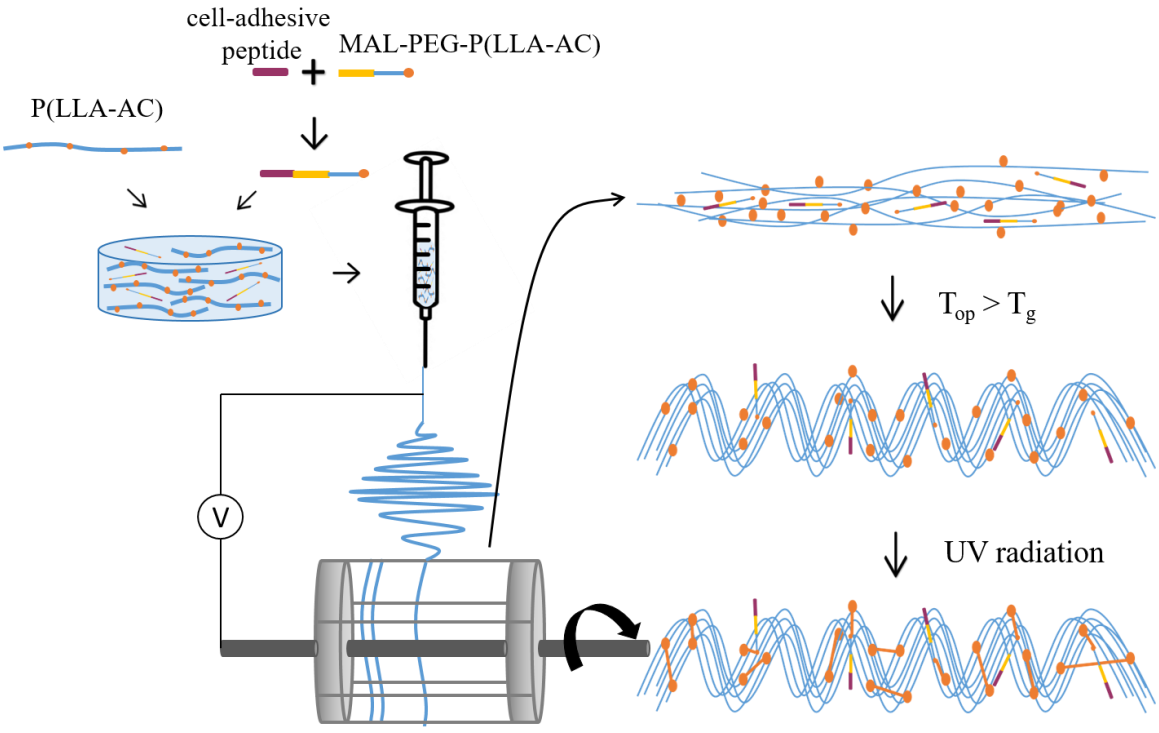

Figure 5: Schematic depicting the fabrication of the biomimetic electrospun polymer fibre scaffolds. Adapted from Chen *et al*.[90]

4.2.1 Materials

All polymers used were prepared in the lab, as described in the previous section. DCM and DMF were obtained from ThermoFisher Scientific (MA, USA), and phosphate buffered saline (PBS) and Irgacure 2959 were obtained from Sigma-Aldrich (MO, USA).

4.2.2 Electrospinning

4.2.2.1 Solution preparation

P(LLA-AC) (300 mg) was placed in a 20 mL glass screw top vial, and photoinitiator Irgacure 2959 (I2959) was added in an amount of 1 w/w% (3 mg). For peptide conditions, 5 w/w% of RGD-conjugated MAL-PEG-P(LLA-AC) (15 mg) was also added to the vial. The sample was dissolved with constant mixing at a concentration of 30 w/v% in a 3:1 DCM:DMF solvent mixture (1 mL), and loaded into a 1 mL disposable syringe immediately before use.

4.2.2.2 Apparatus setup

The electrospinning apparatus consisted of a syringe pump (KD Scientific Inc., USA), high voltage generator (Gamma Voltage Research, USA), and rotating aluminum wire mandrel collector. Samples were loaded in a 1 mL disposable syringe, attached to a blunt-tipped 21G needle using ~50 cm of Tygon chemical-resistant tubing. The wire mandrel, made by attaching two end pieces (~5 cm diameter) to four 10 cm parallel rods, was mounted horizontally to an in-line mixer (Barnart, series 20); a contact tachometer (Extech) was used to measure the rotational speed of the mandrel. The blunt-tipped needle was mounted using a retort stand, and attached to the positive lead of the voltage source. The ground lead was attached to a square piece of aluminum, placed underneath the mandrel. The needle, mandrel, and ground were positioned within an acrylic box to minimize any effects from

surrounding metal objects on the charged polymer stream. Electrospinning parameters used were a set flow rate of 0.03 mL/minute, 17 cm air gap, positive 1 kV/cm electric field, and mandrel rotation speed of 1000 rpm.[90] After electrospinning, the fibres attached to the mandrel were allowed to dry in a fumehood overnight. They were then transferred (still on the mandrel) to a room temperature vacuum desiccator, and further dried, protected from light, for 2-3 days. Fibre mats were then cut from the mandrel, maintaining the largest possible surface area using the fibres that collected between the wires.

4.2.3 Fibre crimping

Fibre mats were transferred to 60 mm diameter glass petri dishes, and placed in an oven at 65 °C for 30 min to induce crimping. Fibre crimp was observed macroscopically with the naked eye, and further visualized using SEM.

4.2.4 Crosslinking

A 400 mL beaker of water was heated to 80 °C in preparation for crosslinking. The UV light source (EFOS 3000, EXFO Canada) was set up so that an intensity of 100 mW/cm^2 was measured at the surface of the water, with a wavelength centred at 365 nm. After crimping, the glass petri dish containing the fibre mat was floated on top of the heated water, and the UV light source was turned on. Samples were irradiated for 15 min on each side. Crosslinking was confirmed by placing samples in DCM, whereupon no dissolution was observed. Scaffolds were stored in a dessicator at room temperature until further use.

4.2.5 Scaffold geometry

After the crimped, crosslinked scaffolds were prepared, they were cut into appropriate geometries for different tests. For mechanical testing and bioreactor studies, samples were cut into rectangles measuring 2.5 x 1.5 cm, with the long cut parallel to the direction of

fibre alignment. For cell attachment studies, discs were cut using a 6 mm diameter biopsy punch.

4.2.6 Characterization

4.2.6.1 SEM

Fibre alignment and crimp were observed under SEM using a JSM-840 Scanning Microscope with a 10 kV electric field and a tungsten filament. Small sections of the scaffold were cut from the fibre mat (after electrospinning and before/after crimping), and mounted on an aluminum stub using double-sided tape. The samples were gold coated using a Hummer VI-A pulse - sputter coating system (Anatech Ltd.) under a 60 mtorr vacuum, prior to SEM imaging.

ImageJ (National Institutes of Health) was used to analyse the SEM images. Fibre diameters were calculated using the measure tool to determine the number of pixels across the width of the fibres in the images, and compared to the length of the scale bar, in pixels. Greater than 20 measurements were performed for each image, sampling a range of fibre diameters. Scaffold porosity was calculated by differentiating between fibres and void space; images were converted to 8-bit and the threshold was adjusted so that fibres were white while the void space was black. The image was made binary, after which a histogram was produced, counting the number of black and white pixels. The porosity was calculated as the number of black (void space) pixels, divided by the total number of pixels in the image.

4.2.6.2 Mechanical testing

4.2.6.2.1 Dynamic/cyclic resilience testing

Cyclic resilience of the samples was tested prior to cell attachment, using a CellScale MCT6 bioreactor (CellScale, ON, Canada). 2.5 x 1.5 cm fibre mats were rolled up along the long edge, and a piece of parafilm was folded over each end to protect the sample from the sharp edge of the grips. Samples were screwed into the bioreactor, after which it was filled with deionized water and allowed to equilibrate at 37 °C. The length of sample exposed between the grips was measured using digital calipers (Mastercraft, USA) for strain calculations. Scaffold samples were tested with various dynamic stretching programs, using MechanoCulture software (CellScale, ON, Canada), ranging from 1 – 10% strain, 0.5 – 1 Hz, and 40 – 64800 cycles.

4.2.6.2.2 Uniaxial tensile tests

Samples were tested under uniaxial tensions using a TA XTplus micromechanical tester (TA Instruments, USA), to understand the mechanical properties and behaviour of the material. 2.5 x 1.5 cm rectangular fibre mats were weighed prior to analysis. The scaffolds were hydrated in PBS for 30 min, then rolled up, maintaining fibre alignment along the long edge of the samples. A small piece of parafilm folded over the ends of the construct, to avoid tearing when exposed to the grips. After immobilization of the sample, the load cell was positioned so as to remove any visual slack in the sample, and data recording commenced after a distance of 0.01mm to avoid recording data corresponding to the removal of slack. The gauge length of the sample was measured using digital calipers (Mastercraft, USA) for strain calculations. Measurements were performed at a rate of 1% strain/s up to 10% strain,[90] or to failure, using Exponent software (Stable Micro Systems,

UK) to acquire distance and load values. Using the initial measurements of the scaffold, the distance-force measurements were converted to strain and stress using the following equations.[89] Tensile stress in the fibres (σ) was calculated as the measured force (F) normalized to the total cross-sectional area of the fibres in the scaffold (A), and displayed in MPa:

$$\sigma = \frac{F}{A}$$

The cross sectional area was calculated using the mass of the scaffold (m), density of poly(L-lactide) (ρ=1.3 g/mL), [129] and the length of the entire scaffold (L_s):

$$A = \frac{m}{\rho L_s}$$

The applied strain (ε) was calculated as the measured deformation ($L-L_0$) normalized to the gauge length of the scaffold (L_0), and displayed as a percentage.

$$\varepsilon = \frac{L - L_0}{L_0}$$

The Young's modulus for the scaffolds was recorded as the slope of the linear region on the resulting stress-strain curves. A trendline was drawn for the linear region before and after the toe region on the curve; the length of the toe region was calculated as the difference between 0% strain and the intersection of the two trendlines.

4.3 Biological Analysis

4.3.1 Materials

All materials were used as received, unless otherwise noted. All materials used in the biological analysis, unless otherwise stated, were obtained from Sigma-Aldrich (MO, USA). Fetal bovine serum (FBS), formic acid, sodium hydroxide, acetic acid, perchloric

acid, HCl, Chloramine-T, and p-dimethylaminobenzaldehyde were all obtained from Thermofisher Scientific (MA, USA). Cell proliferation reagent WST-1 was obtained from Roche (IN, USA), D,L-dithiothreitol was obtained from Fluka Analytical (NJ, USA), and the Quantifluor dsDNA system was obtained from Promega (WI, USA).

4.3.2 Cell isolation

Canadian Council on Animal Care (CCAC) guidelines for the care and use of laboratory animals was observed for all procedures involving animals. Primary ACL fibroblasts were isolated from the midsubstance ligament region of skeletally mature male New Zealand white rabbits. The ACL was excised from the knee under sterile conditions and washed with Hank's Buffered Salt Solution. It was then placed in a solution of Dulbecco's Modified Eagle Medium (DMEM) with 1% Penstrep, and minced with surgical scissors. The minced ACL was digested in a mixture of 5 mg/mL Dispase II and 10 mg/mL collagenase D solution for 75 minutes in a 37 °C shaker, followed by filtration using a 100 μm stainless steel cell sieve. The cells were washed of collagenase using DMEM supplemented with 10% FBS, centrifuged at 1200 x g for 5 minutes, after which the media was aspirated and replaced with 6 mL of DMEM supplemented with 5% FBS and 1% Penstrep. The cells were seeded on 35 mm tissue culture polystyrene (TCPS) petri dishes and cultured to confluence, then passaged and transferred to T-175 flasks. Cells were cultured to confluence with media changes every 2-3 days, using DMEM supplemented with 10% FBS and 1% Penstrep. After passage 2, the cells were frozen down to -80 °C until needed for further studies.

4.3.3 Scaffold sterilization

All polymer scaffolds were sterilized in a biological safety cabinet prior to use with cells. Scaffolds were first sterilized with an ethanol (EtOH) gradient; 100% EtOH for 30 minutes, 85% EtOH for 30 minutes, 70% EtOH overnight, followed by UV irradiation for 30 minutes. The samples were then transferred to PBS, and allowed to equilibrate overnight at 37 °C, 5% CO_2.

4.3.4 Cell attachment study

ACL fibroblast attachment was compared for scaffolds electrospun with and without the inclusion of the peptide-conjugated polymer.

4.3.4.1 Cell attachment to discs

Sterilized 6 mm diameter discs were transferred to 100 mm glass petri dish (one dish per condition, separating ±RGD and ±serum), ensuring that the samples were flattened so the entire surface area was exposed. ACLFs were thawed, counted, and suspended in media with 1% Penstrep (either serum-free, or supplemented with 10% FBS) at a concentration of $4.24x10^5$ cells/mL. 20 µL of the cell suspension was carefully pipetted onto the middle of each disc, for a cell density of $3x10^4$ cells/cm^2. Scaffolds were kept in the biological safety cabinet for 15 min to allow for sufficient attachment, then placed in the incubator at 37 °C, 5% CO_2. After 4 h, the petri dishes were filled with 10 mL complete media (supplemented with 1% Penstrep, 10% FBS), and returned to the incubator.

4.3.4.2 WST-1 assay for cell proliferation

After 24 h, the scaffolds were transferred to 96-well plates, and covered with 100 µL of media and 10 µL of WST-1 dye solution. Concurrently, a cell standard curve (ranging from 0 – 12 000 cells) was seeded on the same 96 well plate, with each well containing 100 µL

of media and 10 µL of WST-1 dye solution. Samples were incubated at 37 °C for 4 h, following which the media from each well was transferred to another 96 well plate. The samples were read using an Enspire Multimode Plate Reader (Perkin Elmer, MA, USA), measuring absorbance at 480 nm, with background correction read at 600 nm.

4.3.4.3 dsDNA quantification using Quantifluor dsDNA system

After the media and WST-1 solution was removed, the wells were rinsed with 100 µL of PBS, and replaced with 100 µL of papain buffer. The edges of the well plate were taped to avoid sample evaporation, and the plate was placed in a 65 °C oven for 18 h. The next day, standards were prepared using the Quantifluor dsDNA system. 1X Tris-EDTA (TE) buffer was prepared by diluting 1 mL of 20X TE buffer with 19 mL nuclease-free water. The standard curve stock was diluted with 20 µL in 980 µL of buffer, for a concentration of 2 ng/µL. Standard samples were made with concentrations ranging from 0 – 2000 ng/mL. The Quantifluor dsDNA dye working solution was diluted 1:200 in 1X TE buffer. After 18 h for cell lysing, each 100 µL sample and 100 µL of each standard (in triplicate) were transferred to a black flat-bottomed 96 well plate. 100 µL of the diluted dye was added to each well, and the assay was incubated for 5 min at 37 °C, protected against light. The fluorescence of the samples was measured with an excitation wavelength of 504 nm and an emission wavelength of 531 nm using an Enspire Multimode Plate Reader (Perkin Elmer, MA, USA). The fluorescence of the blank samples was subtracted from the other samples. A standard curve was plotted using the standard values, and used to calculate the concentration of dsDNA in each unknown sample. The mass of dsDNA in each sample was calculated by accounting for the dilution of the samples, and the original sample volume. The mass of dsDNA per scaffold values were converted to cell number for

comparison with the WST-1 assay. This was done by dividing the mass per scaffold by 5.5 pg of dsDNA per cell,[130] resulting in a value for cell number per scaffold.

4.3.5 Bioreactor study

Four conditions were used for a primary analysis into the effect of dynamic culture for ACLFs on the scaffolds; dynamic culture ± RGD peptide, and static culture ± RGD peptide.

4.3.5.1 Cell attachment to scaffolds

Sterilized 2.5 x 1.5 cm rectangular scaffolds were transferred to four 100 mm glass petri dishes (one per condition), ensuring that the samples were flattened so the entire surface area was exposed. ACLFs were thawed, counted, and suspended in complete media at a concentration of $3.75x10^5$ cells/mL. 300 μL of the cell suspension was carefully pipetted onto the middle of each scaffold, for a cell density of $3x10^4$ cells/cm^2. Scaffolds were kept in the biological safety cabinet for 15 min to allow for sufficient attachment, then placed in the incubator at 37 °C, 5% CO_2. After 4 h, the petri dishes were filled with 10 mL complete media, and returned to the incubator. Cells were allowed to attach to the scaffolds under static conditions over a period of 5 days, with the media changed every second day.

4.3.5.2 Transfer scaffolds to bioreactor

Using sterile surgical gloves and forceps, scaffolds were rolled up along the long edge, with the cells inside of the construct. For the dynamic conditions, scaffolds were transferred to a CellScale MCT6 bioreactor (CellScale, ON, Canada), and screwed into place. Two bioreactors were used for the study; one for scaffolds with RGD and one for scaffolds without. For static conditions, the rolled constructs were transferred to a clean 100 mm glass petri dish. Complete media was added; 125 mL in the bioreactors and 25 mL in the

static petri dishes. The scaffolds were allowed to equilibrate for 24 h prior to their exposure to dynamic conditions.

4.3.5.3 Bioreactor conditions

The bioreactors were programmed to apply a 10% strain at a frequency of 1 Hz, and turned on for 1 h every 24 h. Every second day, the media was aspirated from both the static and dynamic conditions, and replaced with complete media (100 mL dynamic, 25 mL static), to cover the samples. After the 12 days, samples were removed from the bioreactors/ petri dishes, and either fixed in glutaraldehyde for SEM or digested in papain to run assays on the ECM composition.

4.3.5.4 Papain digestion

A digestion buffer was made by dissolving ammonium acetate (0.272 g), 35% EDTA (0.038 g), and D,L-dithioreitol (0.031 g) into 100 mL of milliQ water. The pH of the solution was adjusted to 4 using acetic acid and sodium hydroxide. Immediately before use, papain stock was diluted in the buffer solution to a concentration of 40 μg/mL. The scaffold samples were transferred to 1.5 mL Eppendorf tubes, and covered in 300 μL of the papain digestion solution. Samples were heated to 65 °C for 72 h, with vortexing every 24 h. Samples were then transferred to a -20 °C until required for further analysis.

4.3.5.5 Mass of scaffolds

The mass of a labelled 2 mL Eppendorf tube was recorded for each sample. The scaffolds were transferred to the tubes, rinsing twice with deionized water to remove residual buffer and salts. The samples were frozen in liquid nitrogen and lyophilized over a period of 48 h. The tubes were then re-weighed to calculate the dry mass of the scaffolds.

4.3.5.6 dsDNA quantification

dsDNA was quantified in the scaffolds using the QuantiFluor dsDNA System (Promega). A 1X TE buffer was prepared by dilution 750 µL of the 20X TE stock buffer into 14.25 mL nuclease-free water. The standard curve stock was diluted with 20 µL into 980 µL of buffer, for a concentration of 2 ng/µL. Standard samples were made with concentrations ranging from 0-2000 ng/mL. The Quantifluor dsDNA dye working solution was diluted 1:200 in 1X TE buffer. Unknown samples were diluted with 5 µL into 495 µL of papain digestion buffer. Using a black flat-bottomed 96 well plate, 100 µL of each diluted sample or standard was added to the wells in triplicate. 100 µL of the diluted dye solution was added to each well, and the assay was incubated for 5 min at 37 °C, protected against light. The fluorescence of the samples was measured with an excitation wavelength of 504 nm and an emission wavelength of 531 nm using an Enspire Multimode Plate Reader (Perkin Elmer, MA, USA). The fluorescence of the blank samples was subtracted from each other sample. A standard curve was plotted using the standard values, and used to calculate the concentration of dsDNA in each unknown sample. The mass of dsDNA in each sample was calculated by accounting for the dilution of the samples, and the original sample volume.

4.3.5.7 Hydroxyproline assay for collagen quantification

The collagen content in each scaffold sample was quantified using a hydroxyproline (OHP) assay. 100 µL of each papain-digested sample was transferred to glass test tube with a Teflon-lined screw cap. To each, 100 µL of 12 N HCl was added, followed by incubation on a heating block at 110 °C for 22 h. The hydrolysate was neutralized with 100 µL of 5.7 N NaOH. Following neutralization, the samples were transferred to 1.5 mL Eppendorf

tubes, and activated charcoal (10 mg) was added to each sample. Samples were vortexed then centrifuged for 3 min at 10000 x g. The supernatant was removed and transferred to a clean Eppendorf tube, and stored at -20 °C overnight, prior to assaying.

An acetate-citrate buffer (pH 6) was made by mixing sodium acetate (7.23 g), citric acid (5 g), sodium hydroxide (3.4 g), and glacial acetic acid (1.2 mL) into 100 mL dH_2O. Perchloric acid (3.15 N) was prepared by dilution 70% perchloric acid (4.6 mL) into dH_2O (14.6 mL). Chloramine-T solution (0.05 N) was prepared by mixing Chloramine-T (141 mg), dH_2O (2 mL), 2-methoxyethanol (3 mL), and the previously prepared acetate citrate buffer (5 mL). Finally, Ehrlich's reagent was prepared by dissolving p-dimethylaminobenzaldehyde (1 g) into 5 mL 2-methoxyethanol, and heating it at 60 °C for 20 min. Hydroxyproline standards were prepared with concentrations ranging from 0-5 μg/ml from a 100 μg/mL stock in dH_2O.

For the assay, 50 μL of the standards and samples were pipetted in triplicate in a 96-well plate. 50 μL of the 0.05 N Chloramine-T solution was added to each well, and allowed to mix for 20 min. Next, 50 μL of 315 N perchloric acid was added to each well, and left for 5 min. 50 μL of Ehrlich's reagent was added to each well, then the plate was heated at 60 °C for 20 min. The plate was transferred to a 4 °C fridge for 5 min, and then allowed to stabilize at room temperature for 30 min. The absorbance of the samples was read using an Enspire Multimode Plate Reader (Perkin Elmer, MA, USA), at 560 nm. For calculations, the absorbance of the blank samples was subtracted from all sample and standard measurements. A standard curve of OHP concentration and absorbance was plotted using

the standard curve measurements, and used to calculate the concentration of all unknown samples. Accounting for the dilution and initial volume of unknown samples, the mass of OHP was calculated and converted to the mass of collagen using a 1:7.64 ratio of OHP:collagen.

4.3.5.8 DMMB assay for GAG quantification

The quantity of sulfated glycosaminoglycans (GAG) in each scaffold was calculated using the DMMB assay. The DMMB dye solution was first prepared. 500 mL of 0.2% formic acid was prepared by diluting 88% formic acid (1.135 mL) into dH_2O (498.865 mL). The acid was then titrated to pH 1.5 using concentrated formic acid. DMMB dye (10.5 mg) was dissolved in 100% ethanol (2.5 mL), then mixed into the pH 1.5 formic acid (497.5 mL). To make a working stock of 1 mg/mL for the standards, the 10 mg/mL chondroitin sulfate sodium salt stock (100 μL) was diluted in papain digestion solution (900 μL). Standards were prepared with chondroitin sulfate concentrations ranging from 0-60 μg/mL.

To run the assay, 40 μL of each sample or standard was pipetted in triplicate into a clear flat-bottom 96-well plate. 125 μL of DMMB dye was added to each well, and briefly mixed. The absorbance of each sample was measured using an Enspire Multimode Plate Reader (Perkin Elmer, MA, USA) at 525-595 nm. For calculations, the samples were corrected by subtracting the blank absorbance. A standard curve of chondroitin sulfate concentration and absorbance was plotted. Using the standard curve equation, the concentration of all unknown samples could be calculated. Accounting for dilution and initial volume, the mass of GAG in each sample was calculated.

4.3.6 Statistics

Significant differences were assessed using a one-way ANOVA with Tukey's post hoc test performed using Graphpad Prism 7 (Graphpad Software, CA,USA), with $p \leq 0.05$ considered significant ("*"= $p < 0.05$, "**"= $p < 0.01$). Unpaired t-tests were performed when appropriate. Data values are presented as mean ± standard error, with the sample per group (n) indicated for each experiment.

Chapter 5

Results and discussion

5.1 Polymer Preparation

5.1.1 Synthesis of acryloyl carbonate (AC)

The acrylated TMC monomer (AC) was successfully synthesized, confirmed by ^{1}H NMR spectral analysis after each of the four steps of the reaction. The final spectrum is shown (Figure 6).

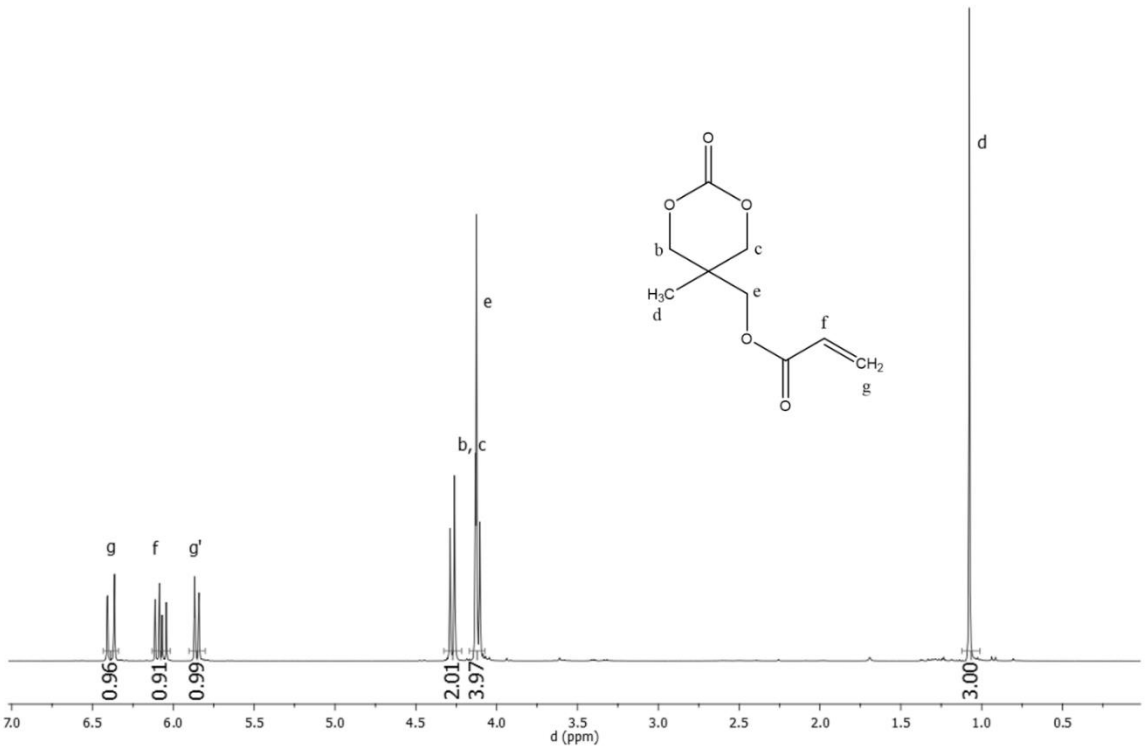

Figure 6: ^{1}H NMR spectrum of the acryloyl carbonate (AC) monomer, showing integration and peak assignment. Sample was run in $CDCl_3$ and at 400 MHz.

In order to improve the overall yield of the synthesis, the third step of the reaction was optimized. Initially, the deprotection reaction was performed at 60 °C, with dilute HCl (1 M) over 3 h, which resulted in yields of less than 30%. Based on observations from the ^{1}H NMR spectra, it appeared that water in the reaction was cleaving the pendant acryl group, while the deprotection was occurring, resulting in the production of 2,2-dimethoxypropane, acetone, and acryloyl chloride, essentially reverting to the initial reagents of the synthesis. To remedy this, and improve the overall yield of the synthesis, the conditions were altered. First, the reaction was attempted with a heterogeneous $NaHSO_4 \cdot SiO_2$ catalyst at room temperature, to avoid the introduction of water into the system and simplify the purification process. On occasion this process improved the yield of the reaction (>60%); however, it was inconsistent, and usually little to no deprotection was observed. The other method involved using a stronger acid (12 M HCl) to reduce the amount of water in the system, and milder reaction conditions (addition of acid and neutralization at 0°C, reaction allowed to proceed at room temperature) to avoid cleavage. This method consistently improved the yield to greater than 70%, and was used in all future AC synthesis reactions.

5.1.2 Synthesis of P(LLA-AC)

L-lactide and AC monomer were successfully co-polymerized using $Sn(Oct)_2$ as a catalyst and 1-octanol as an initiator. ^{1}H NMR spectroscopy was used to confirm the structure and purity of the polymer, as well as to determine the AC content in the copolymer (Figure 7).

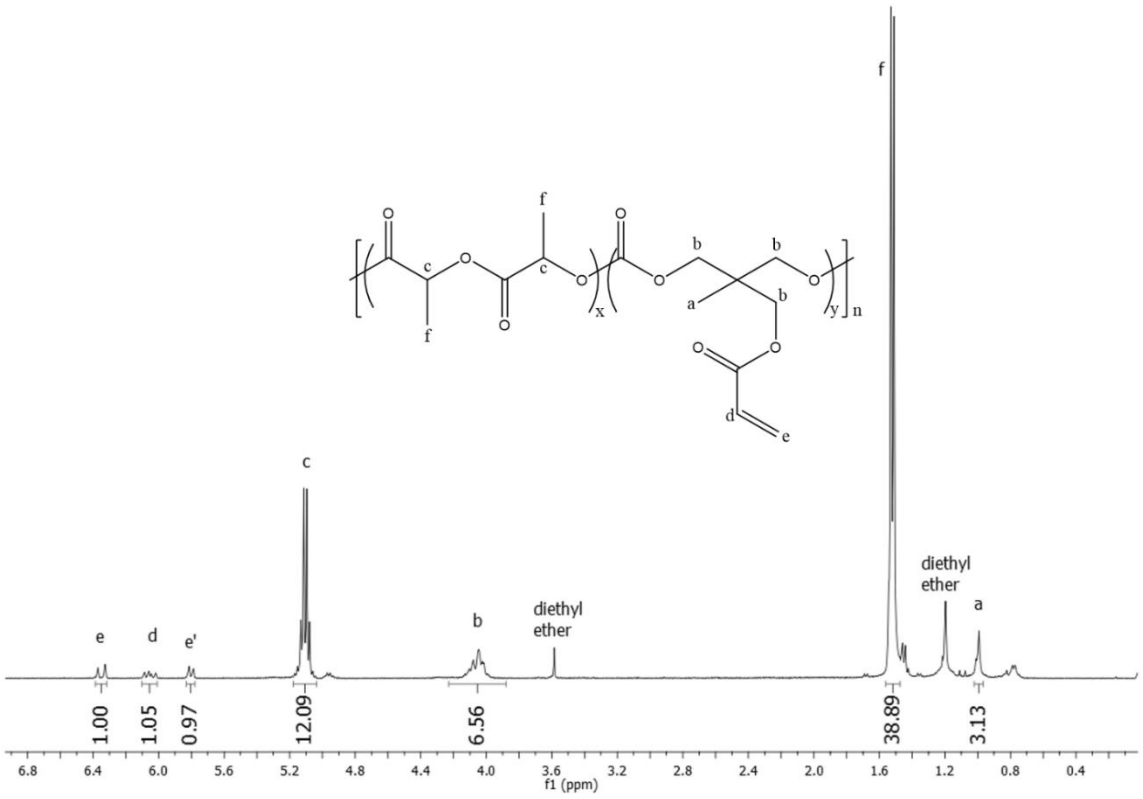

Figure 7: ^{1}H NMR spectrum of synthesized P(LLA-AC) copolymer prepared with 1000:1 monomer: initiator, showing integration and peak assignment. Sample was run in $CDCL_3$ and at 400 MHz.

The AC content was calculated by comparing the integration of the area under peaks in the AC monomer to the lactide monomer. For the calculation, peaks d, e, and e', corresponding to the vinyl protons on the pendant acrylate were compared to peak c, the methine proton along the lactide backbone. Equation (1) shows the calculations performed for the spectra in Figure 7.

$$AC\ content = \frac{\sum Integration(d,e)/3H}{Integration(c)/2H} = \frac{3.02/3}{12.09/2} = 16.7\% \quad (1)$$

With a target of 20% AC, the resulting polymer had an AC content of 16.7%, consistent with previous results.[90] The low AC content compared to the target was previously

hypothesized to be due to lower reactivity of the AC monomer than the lactide monomer, likely as a result of the bulky pendant acrylate group.[90] From GPC analysis, the number average molecular weight (M_n) of the copolymer was approximately 25 kDa.

5.1.2.1 Increased molecular weight

The first polymer with a number average molecular weight of 25 kDa proved difficult to manipulate and remove from the mandrel after electrospinning. To facilitate manipulation, the polymer formulation was modified to increase the molecular weight. While the initial formulation used a monomer:initiator ratio of 500:1, copolymers were synthesized with a ratio of 1000:1, and without initiator. ^{1}H NMR analysis showed that the new formulations had lower, but still comparable AC content to the original, while GPC analysis confirmed that the number average molecular weight increased (Table 1). Based on these results, further electrospinning and analysis were performed using polymers made with no initiator.

Table 1: Comparison of polymer properties based on monomer: initiator feed ratio.

Monomer: Initiator	AC content (^{1}H NMR)	M_n (kDa, GPC)
500:1	16.7%	25
1000:1	11.5%	38
No Initiator	10.9%	48

5.1.3 Synthesis of MAL-PEG-P(LLA-AC)

A MAL-PEG-P(LLA-AC) copolymer was also synthesized to use for peptide conjugation using maleimide-PEG as the initiator. The maleimide functionalization allows for Michael

addition with the cysteine residue of the peptide, while the PEG component was added to improve the solubility of the conjugate in the solution used for electrospinning. The structure of the polymer was confirmed via ^{1}H NMR analysis, which demonstrated the presence of the vinyl protons on the maleimide (peak h) and the vinyl protons on the pendant acrylate groups (peaks d and e) (Figure 8).

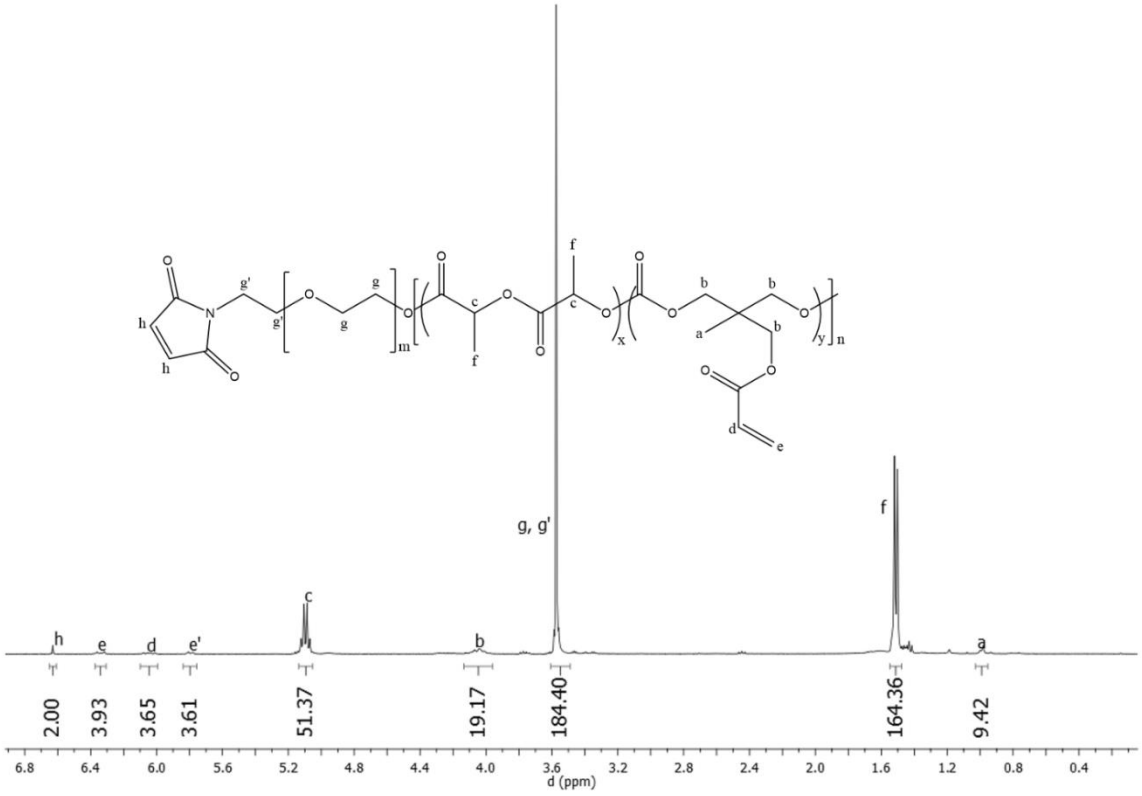

Figure 8: ^{1}H NMR spectrum and peak assignments, confirming the successful synthesis of the MAL-PEG-P(LLA-AC) copolymer. $CDCl_3$, 400 MHz.

Using Equation (1), as above with the integrations of the area under peaks d/e and c, the acrylate content was calculated as 14.5%, from a target of 20%. The molecular weight of the sample was determined by calculating the number of repeating units of each monomer,

multiplying by the respective molecular weights and calculating the sum, as shown in the following equations:

Lactide: compare methine backbone peak ‘c’ (2H) to PEG methylene peak ‘g’ (4H).

$$n = \#\ PEG\ units = 45, m = \#LLA\ units$$

$$m = n * \frac{Integration(c)/2H}{Integration(g)/4H} = 25$$

Acrylate: compare sum of vinyl proton peaks ‘d, e’ (3H) to PEG methylene peak ‘g’ (4H).

$$n = \#\ PEG\ units, p = \#\ AC\ units$$

$$m = n * \frac{\sum Integration(c)\ /3H}{Integration(g)/4H} = 3.6$$

$$MW = Mn_{PEG} + M_{LLA} * m + M_{AC} * p = 6323\ Da$$

The polymer was successfully synthesized with a maleimide functional group, an acrylate content of 14.5% which was comparable to the bulk polymer, and a molecular weight of 6.3 kDa. Additionally, the polymer was soluble in the 3:1 DCM:DMF electrospinning solution with the inclusion of the maleimide and PEG spacer, which was the first step in being able to dissolve the peptide for electrospinning.

5.1.4 Synthesis of GPSDGRGYGCG peptide

The GPSDGRGYGCG peptide was synthesized in the lab, and its molecular weight confirmed using MALDI-TOF analysis, expecting a molecular weight of 1025.06 Da. An early batch of peptide also had a large peak at 1277 Da, which was hypothesized to be due to the (pentamethyl-2,3-dihydrobenzofuran-5-sulfonyl (pbf) protecting group on the arginine residues (MW = 252 Da). Literature shows that arginine protecting groups, including pbf can be difficult to remove and require longer deprotection times.[131] To overcome this, the time that the peptide was exposed to the deprotection cocktail was

doubled from 60 min to 120 min. After this alteration to the process, consequent MALDI spectra did not show major peaks at 1277 Da, indicating that the longer deprotection times were successful in removing the pbf group. Due to the impurities observed with mass spectroscopy, HPLC was used to further purify the synthesized peptide. After purification of the peptide the MALDI-TOF showed a much cleaner spectrum (Figure 9), with one major peak at the desired molecular weight (1025 Da).

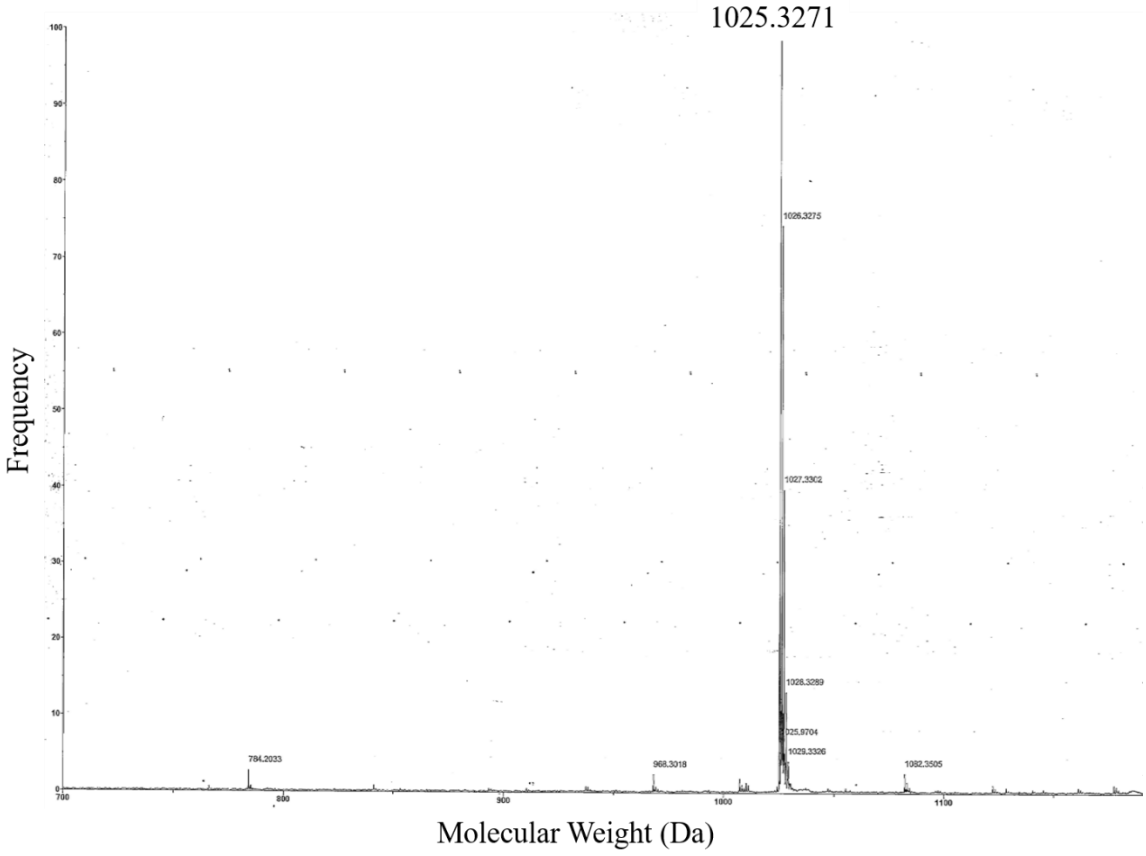

Figure 9: MALDI-TOF spectrum showing GPSDGRGYGCG peptide after HPLC purification.

5.1.5 Conjugation of peptide to MAL-PEG-P(LLA-AC)

Figure 10 shows a schematic representation of the Michael-type addition reaction between the thiol of the cysteine residue on the peptide and the maleimide functional group on the polymer.

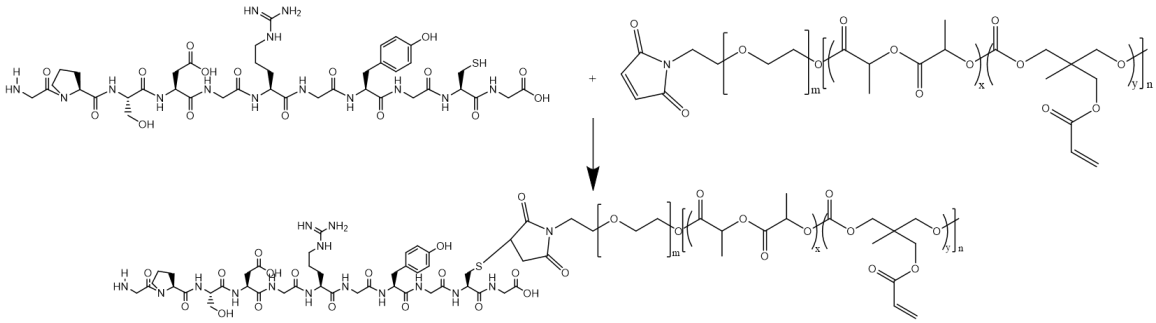

Figure 10: Schematic representation depicting the Michael-type reaction resulting in the conjugation of the GPSDGRGYGCG peptide to the MAL-PEG-P(LLA-AC) polymer.

The conjugation of the GPSDGRGYGCG peptide to the MAL-PEG-P(LLA-AC) polymer was observed using ^{1}H NMR (Figure 11). The spectrum shows that the peaks corresponding to the vinyl group of the acrylate (5.75-6.5 ppm) were conserved in an appropriate area ratio compared to the other polymer peaks. The peak at 6.6 ppm, corresponding to the vinyl protons of the maleimide group, clearly visible in Figure 8, completely disappeared, indicating a loss of the maleimide functionality due to conjugation of the peptide. This analysis was used to confirm the conjugation of peptide to the polymer at the maleimide functional group, rather than at the acrylate.

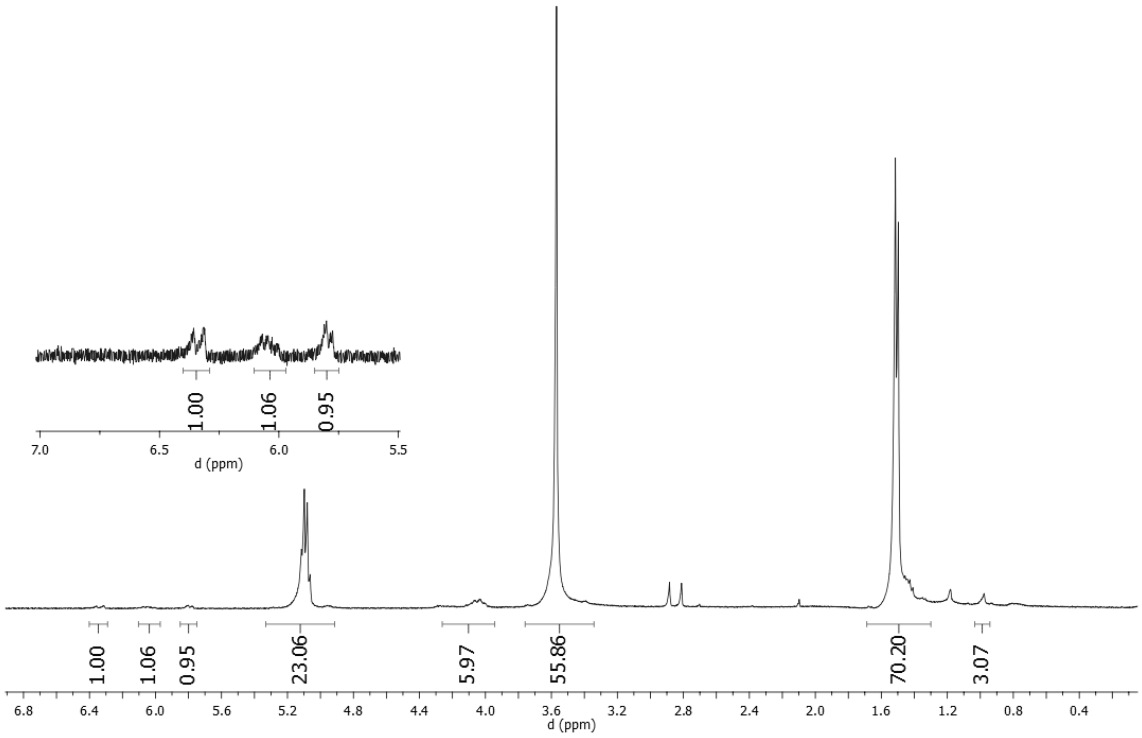

Figure 11: ^{1}H NMR spectrum showing conjugation of GPSDGRGYGCG peptide to MAL-PEG-P(LLA-AC) in the presence of TCEP. $CDCl_3$, 400 MHz.

^{1}H NMR analysis of the polymer, peptide, and conjugate were also run in a 50:50 mix deuterated chloroform and deuterated dimethyl sulfoxide (DMSO) to better visualize the peptide peaks (Figure 12). The peak locations shifted as a result of deshielding due to the change in solvent system; the maleimide peak in the polymer (Figure 12a and d) was observed at 7 ppm instead of 6.6 ppm in the chloroform-d-only spectra. With the inclusion of DMSO, the peptide was more soluble and could be observed both alone and in the peptide-polymer conjugate. The peptide peaks at 6.6 and 7.0 ppm were conserved in the conjugation, as were the vinyl proton acrylate peaks at 5.9-6.4 ppm.

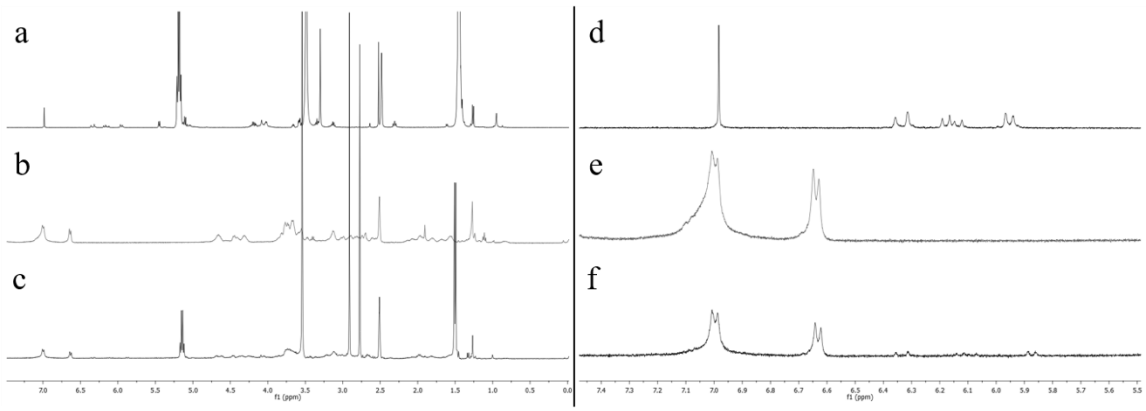

Figure 12: ^{1}H NMR spectra showing polymer-peptide conjugation, with the full spectra shown on the left and a close up of the maleimide / acrylate region on the right. a,d) MAL-PEG-P(LLA-AC), b,e) GPSDGRGYGCG peptide, c,f) peptide-polymer conjugate. 50:50 $CDCl_3$: $(CD_3)_2SO$ mix, 400 MHz.

For initial conjugation reactions, TCEP was used to reduce the possibility of disulfide bond formation between peptide molecules. The TCEP was difficult to remove during the purification of the conjugate, as it also precipitated in diethyl ether. The TCEP also precipitated in the DCM/DMF electrospinning solution, which made it difficult to observe whether the conjugate was soluble. However, the amount of TCEP that precipitated was minute, and it was difficult to remove from the solution. To remedy this issue, conjugation reactions were tested without TCEP. All solutions that the peptide encountered between synthesis and conjugation were purged with inert gas (argon or nitrogen) to reduce oxidation of the sulfide. The conjugation without TCEP was successful, as can be seen in the ^{1}H NMR spectrum in Figure 13, and therefore all ensuing conjugations were performed in purged solutions, without the use of TCEP.

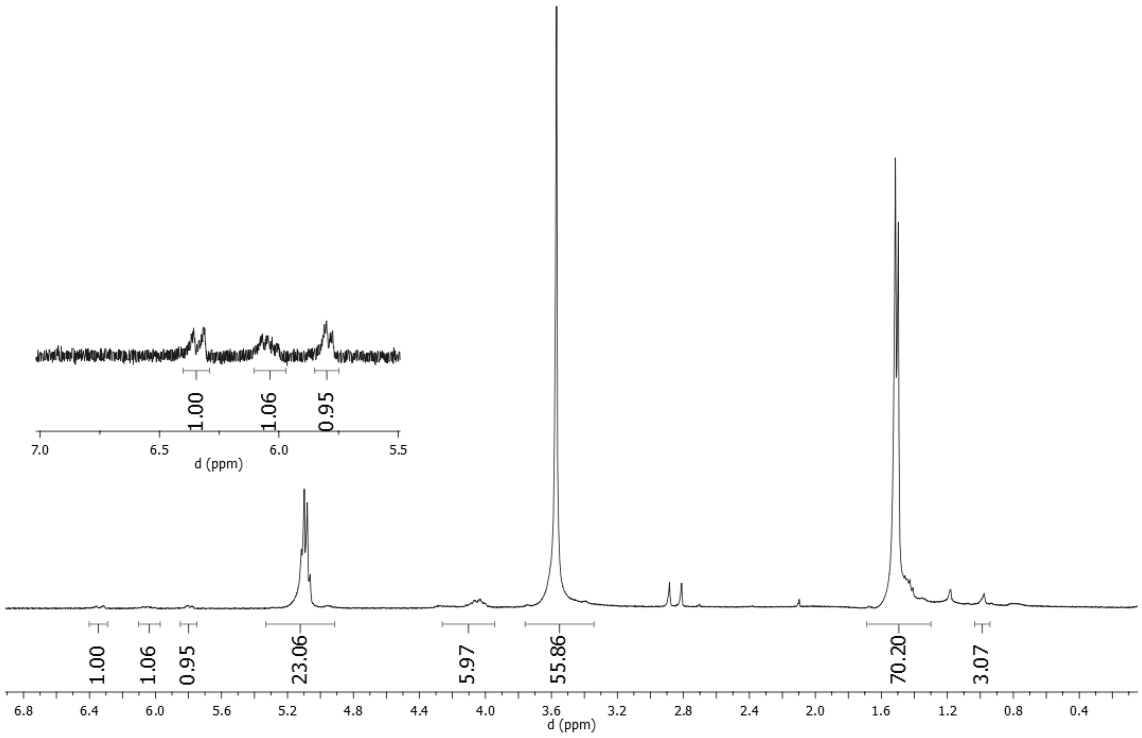

Figure 13: ^{1}H NMR spectrum showing conjugation of GPSDGRGYGCG peptide to MAL-PEG-P(LLA-AC) without TCEP. $CDCl_3$, 400 MHz.

5.2 Scaffold Fabrication

5.2.1 Electrospinning

Both the bulk polymer on its own, and the bulk polymer with the peptide-polymer conjugate, dissolved in the 3:1 DCM:DMF solution, which was the first step in the electrospinning process. The solubility of the peptide-polymer conjugate demonstrated that the PEG was an appropriate length to assist in the dissolution of the hydrophilic peptide. At the chosen concentration of peptide-polymer conjugate (5 w/w%), this method was successful. Additionally, it was at this stage that residual TCEP was observed in the electrospinning system using the peptide-polymer conjugate. This problem was remedied

by eliminating the use of TCEP in the conjugation, as discussed above. After this change, no particulates could be seen in the solution after dissolution of the bulk polymer and peptide-polymer conjugate.

Both systems were successfully electrospun onto rotating mandrels, producing aligned fibrous mats. Throughout the process, electrospinning parameters such as voltage, distance to mandrel, solution concentration, and injection flow rate were varied to improve the alignment of the fibres. The parameters that resulted in aligned fibres and were used in further studies were: a flow rate of 0.03 mL/min, 17 cm air gap, positive 1 kV/cm electric field, and mandrel rotation speed of 1000 rpm, as shown in previous studies.[90] Additionally, an acrylic box was added to the electrospinning set up; housing the needle and collector to insulate the charged polymer stream from the grounding effects of the metal components.

SEM images highlighting the degree of alignment of the resulting fibres are shown for the scaffolds with (Figure 14d-f) and without (Figure 14a-c) peptide. The yellow arrows demonstrate the direction of fibre alignment. While the majority of the fibres were aligned along a main axis, due to the whipping of fibres during the electrospinning process, there were fibres that did not conform. This issue is particularly noticeable in the 100X images. As more polymer fibres are deposited on the mandrel, the residual charge in the fibrous mat increases, and the charged polymer jet is repelled from the mat, causing more whipping. This whipping results in a reduction in fibre alignment on the top layer of the scaffold.

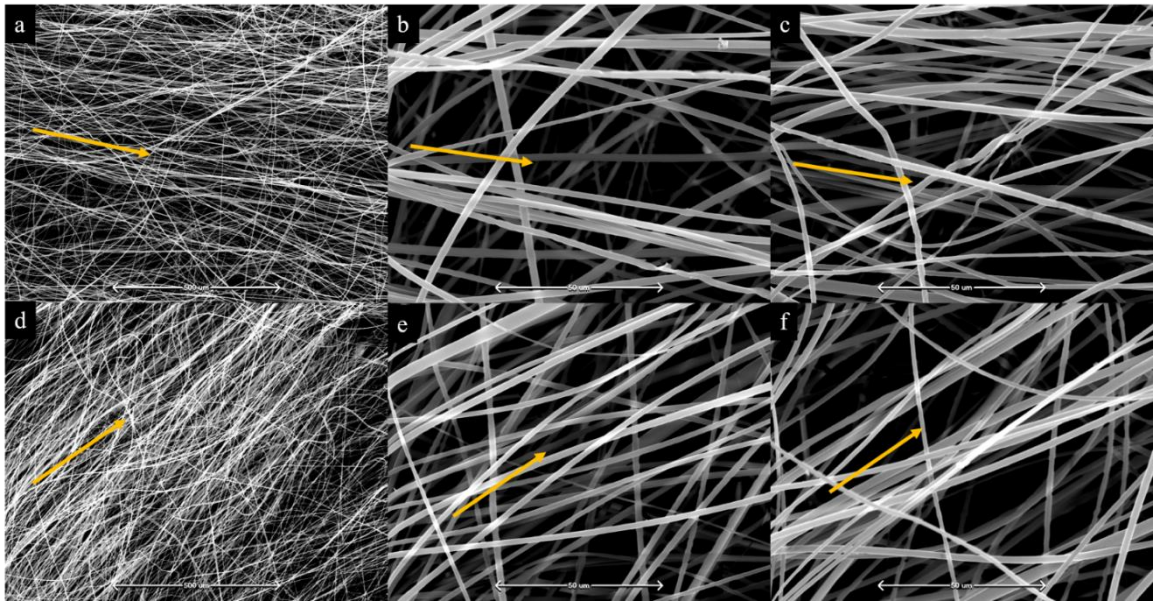

Figure 14: SEM images showing fibre alignment in electrospun scaffolds, made with bulk P(LLA-AC) alone (a-c) and with peptide-conjugated polymer (d-f). Magnification: a, d, 100X; b, c, e, f, 1000X. Arrows show direction of fibre alignment.

Using Image J, the average fibre diameters for each system were measured. The scaffolds made with only the bulk copolymer had an average diameter of 1.13 ± 0.36 μm, while the scaffolds that included the peptide-polymer conjugate had an average diameter of 1.12 ± 0.35 μm. These images and calculations demonstrate that the peptide can successfully be incorporated into the electrospun scaffolds, without significant differences in fibre architecture.

5.2.2 Crimping and crosslinking

The thermal properties of the P(LLA-AC) polymers with molecular weights of 25 and 48 kDa were measured using DSC before and following electrospinning to determine if the peptide or electrospinning solvents affected the glass transition temperature (T_g). Table 2 shows the calculated T_g values for the various samples. While the peptide and

electrospinning had minimal effects on the T_g, the higher molecular weight polymer had an increased T_g, as expected, which had to be taken into account for crimping the fibres. As crimping occurs when $T_{op}>T_g$, all samples were crimped at 65 °C, to ensure T_{op} was approximately 10 °C greater than the T_g, based on the results shown by Surrao *et al.*[104] After the samples have been placed in the oven, the process was apparent as the fibres constricted and the crimp was easily observed without the aid of microscopy.

Table 2: Comparison of glass transition temperatures for bulk and electrospun polymer formulations.

Conditions	M_n (kDa)	T_g (°C)
Bulk Polymer	25	43.9
Electrospun, no peptide	25	46.8
Electrospun, peptide	25	46.0
Bulk Polymer	48	53.4
Electrospun, no peptide	48	54.7

The crosslinking process was also modified to be performed at elevated temperatures, as at ambient temperatures samples did not properly crosslink. The degree of crosslinking was tested by placing the samples in DCM after UV irradiation; crosslinked samples maintained their architecture, while those that did not crosslink dissolved in the solvent. Samples crosslinked at room temperature dissolved, regardless of extended crosslinking times. It was hypothesized that at ambient temperatures, below the copolymer T_g, acrylate functional groups not already in close proximity would be unable to react as the polymer

chains were immobile. However, at $T_{op} > T_g$, chain movement would be possible, meaning that the acrylate functional groups had sufficient mobility and could react. When crimped samples were maintained at the elevated $T_{op} > T_g$ during crosslinking, the process was successful and they did not dissolve when exposed to DCM.

Crimped and crosslinked samples were imaged using SEM to confirm the architecture, and to compare with aligned samples before crimping. Figure 15 shows these images for both the scaffolds made only with the P(LLA-AC) bulk polymer (a-b), and with the inclusion of the peptide-polymer conjugate (c-d). The arrows show the alignment of the fibres, which is conserved through the crimping and crosslinking process.

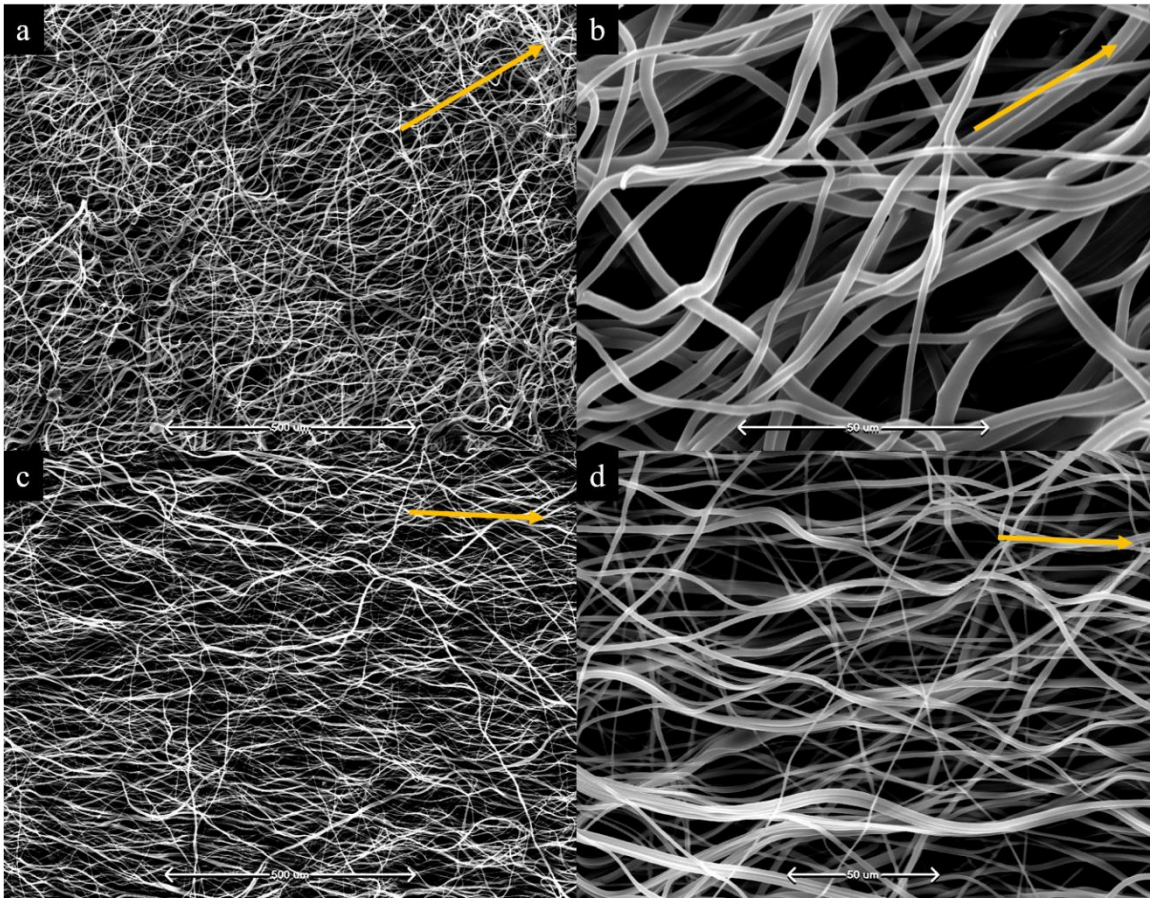

Figure 15: SEM images showing crimped architecture in electrospun fibres, made with bulk P(LLA-AC) alone (a-b) and with peptide-conjugated polymer (c-d). Magnification: a, c, 100X; b, d, 1000X. Arrows show direction of fibre alignment.

ImageJ was used to calculate the porosity of the scaffolds. The bulk-only scaffolds had a porosity of 42.1 ± 4.2%, while those with the peptide-polymer conjugate had a porosity of 42.0 ± 3.5%. These results further demonstrate that the peptide-polymer conjugate can be incorporated into the scaffold without significant effect on the architecture.

5.2.3 Mechanical behaviour

5.2.3.1 Dynamic/cyclic resilience testing

Scaffold samples were placed in the CellScale bioreactor to identify how best to roll and secure them into the bioreactor, prior to sterilization and seeding with ACLFs. Additionally, this process allowed for different dynamic programs to be tested to determine the resiliency of the scaffolds before cell seeding.

In the attempts to position the samples in the bioreactor, it was apparent that if the grips were tight enough that the samples would not slip through, the edge of the grip would tear the sample. The tight grips and subsequent tearing were more likely to cause failure of the samples at the grip edges, rather than at the midpoint of the sample, where it would be expected to fail. To remedy this problem, parafilm was wrapped around the edges of the rolled sample, so that the grips clamped down on the parafilm instead of the sample. While the modification was successful in reducing the number of samples that tore due to the grips, parafilm could not be used with the cell-seeded scaffolds, as it cannot be easily sterilized.

Scaffold samples, first dry then hydrated, were tested in the bioreactor to ensure that they could withstand the desired programs for cell stimulation. Samples were first tested with smaller strain magnitudes and lower frequencies, then the strain magnitude was progressively increased as the samples proved resilient. Table 3 summarizes the range of conditions under which the scaffolds were tested. As the hydrated scaffolds were capable

of sustaining 10% strain at 1 Hz for 18 continuous h, it was assumed there would be no risk in exposing cell-laden scaffolds to these conditions for 1 h per day for 14 days.

Table 3: Summary of conditions that scaffolds withstood in bioreactor.

Strain	Frequency (Hz)	Cycles	Duration	Hydration	Temperature (°C)
1%	0.5	40	1.3 min	dry	25
10%	0.5	40	1.3 min	dry	25
10%	1	150	2.5 min	dry	25
10%	1	150	2.5 min	hydrated	25
10%	1	150	2.5 min	hydrated	37
10%	1	450	7.5 min	hydrated	37
5%	1	10800	3 h	hydrated	37
10%	1	900	15 min	hydrated	37
10%	1	3600	1 h	hydrated	37
10%	1	64800	18 h	hydrated	37

5.2.3.2 Uniaxial tensile testing

Fibre scaffolds, with and without the peptide-polymer conjugate, were tested under uniaxial tensile strain in order to prepare stress-strain curves. The measured values of load and distance, as well as the mass of the scaffolds, were used to calculate stress and strain values,[89] as described in the methodology section. Figure 16 and Figure 17 show the stress-strain curves for all samples for the bulk polymer and peptide-conjugated polymer

scaffolds, respectively. It is important to note that a toe region can be seen on the curves, indicative of the desired biomimetic mechanical behaviour of the materials due to the unfolding of the fibre crimp at low strain values.

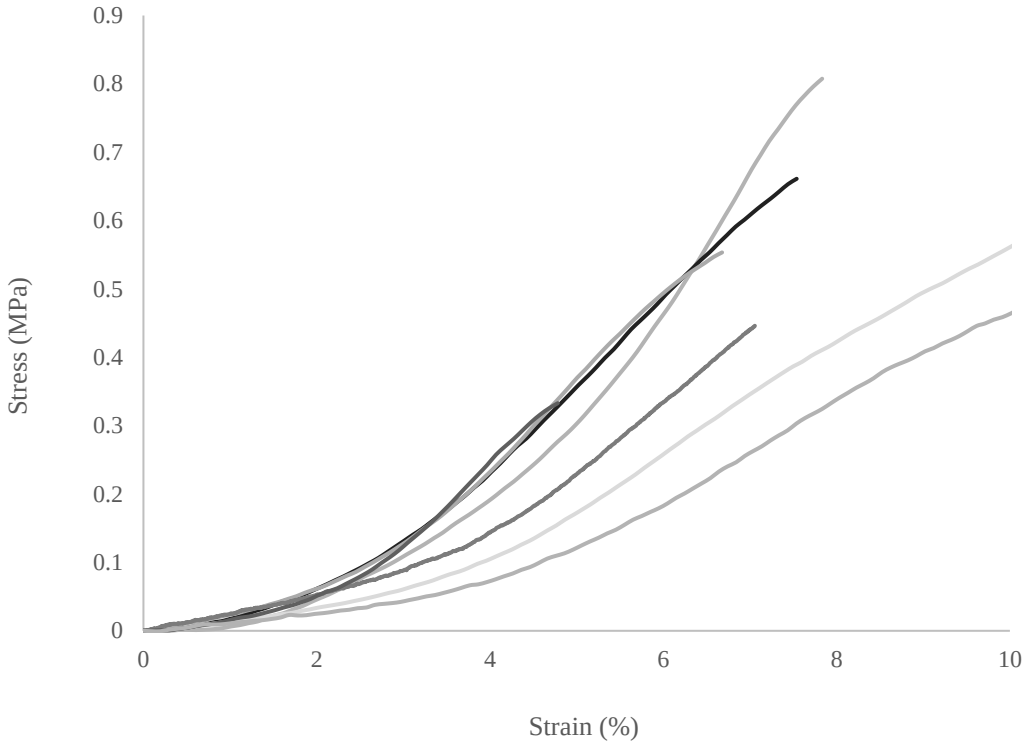

Figure 16: Stress-strain curves for electrospun fibre scaffolds made with bulk P(LLA-AC) copolymer.

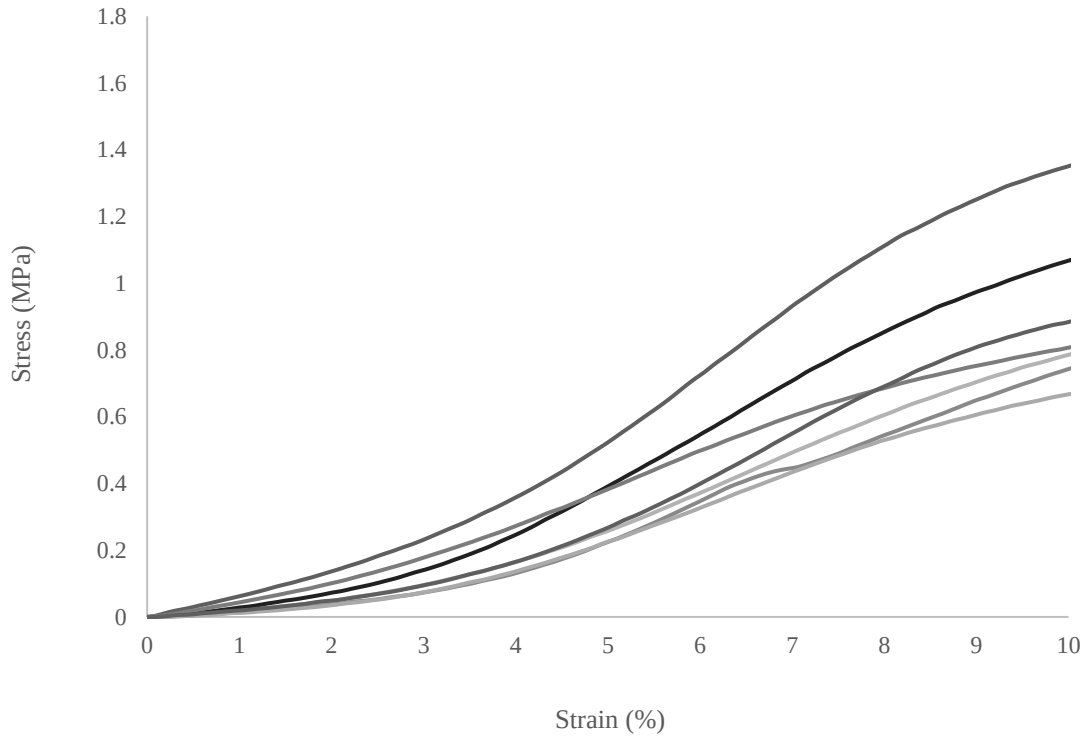

Figure 17: Stress-strain curves for electrospun fibre scaffolds made with bulk P(LLA-AC) copolymer and peptide-polymer conjugate.

The Young's modulus for each sample was calculated by performing regression on the linear portion of the graphs, following the toe region. Figure 18 shows a representative curve, with a trendline indicating the linear region. To calculate the length of the toe region, a trendline was also drawn on the initial linear region of the graph. The length of the toe region is calculated as the difference between 0% strain and the intersection of the two trendlines, and therefore the length of the toe region for this sample is 4.1% strain.

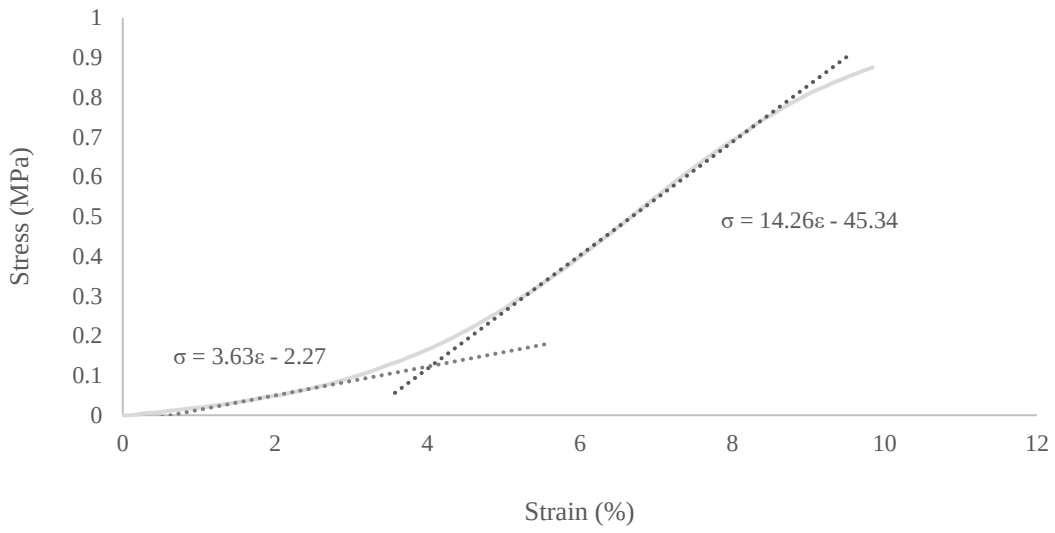

Figure 18: Representative stress-strain curve showing the toe region and linear region, with corresponding linear trend-lines.

Table 4 summarizes the average Young's modulus values for the respective polymer systems, as well as the average length of the toe regions, taken as the distance between zero strain and the onset of the linear portion of the curve.

Table 4: Summary of biomechanical properties for polymer scaffolds, n=7.

	Young's Modulus (MPa)	Toe Region
Bulk P(LLA-AC) copolymer	13.5 ± 1.9	3.7 ± 0.3%
Bulk P(LLA-AC) copolymer + peptide-polymer conjugate	13.9 ± 1.3	3.8 ± 0.1%

Again, the values for the scaffolds including the peptide conjugate are not significantly different to those for the bulk polymer alone, demonstrating that the peptide did not affect

the architecture and mechanical behaviour of the material. These values are lower than the Young's modulus of native ACL tissue, reported by Noyes and Grood as 110 ± 15 MPa[35]. While the hydrated modulus of the synthetic scaffolds is approximately an order of magnitude lower than the native ACL tissues, ideally ECM production in the bioreactor would strengthen the scaffold construct due to increased collagen content, and result in a Young's modulus comparable to native tissue. Unfortunately, there was not enough samples remaining after the bioreactor study to perform mechanical analysis. The length of the toe region for both scaffold types is comparable to those shown by Skelley *et al.*[132] for native ACL, indicating appropriate crimp parameters, and that the crimped architecture of the synthetic scaffolds successfully mimics the tri-phasic stress-strain behaviour in native ACL tissues.

5.3 Biological Analysis

5.3.1 Cell attachment study

To assess the effect of the RGD peptide on cell attachment, scaffold discs were made using both the bulk P(LLA-AC) polymer alone, and the peptide-polymer conjugate blend; a 6 mm biopsy punch was used to cut uniformly sized discs from the crimped, crosslinked, electrospun fibre mats. Using the geometry of the scaffolds, and a suspension droplet volume of 20 μL, cells were suspended at a concentration of 4.24×10^5 cells/mL, which resulted in a seeding density of 8.5×10^3 cells/scaffold (3×10^4 cells/cm^2). Cell number on the scaffolds was measured after 24 h using both the Quantifluor dsDNA assay (Figure 19) and the WST-1 assay (for the number of metabolically active cells, Figure 20a) (no peptide n=6, +RGD n=7). The mass of dsDNA per scaffold values from the Quantifluor assay were converted to cell number per scaffold (Figure 20b).

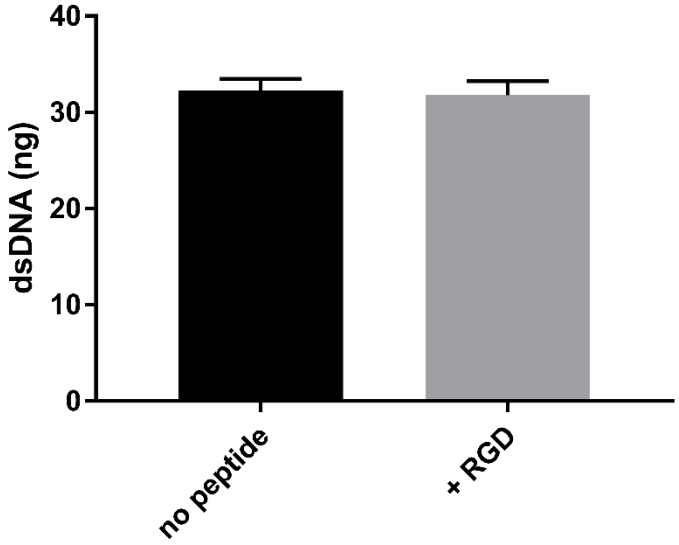

Figure 19: Mass of dsDNA per scaffold comparison for scaffold discs with and without peptide conjugate, using Quantifluor dsDNA assay.

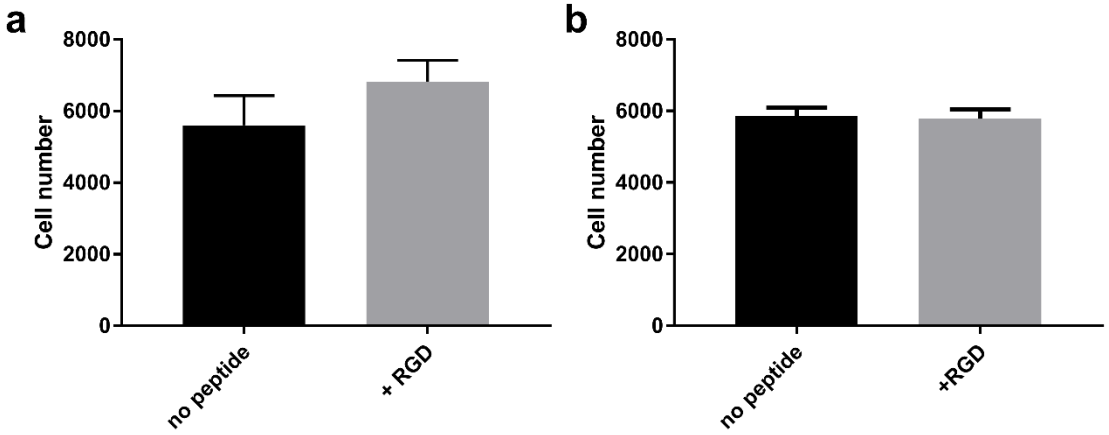

Figure 20: Comparison of number of ACLFs per scaffold for discs made with and without peptide-polymer conjugate, calculated using WST-1 proliferation assay (a) and Quantifluor dsDNA assay (b).

From these results, there was no significant difference in cell attachment to the scaffolds in the presence or absence of the RGD-containing peptide. This result was unexpected, as Wang *et al.*[125] saw an increase in seeding efficiency in the presence of RGD on aligned silk fibres, and the peptide motif is hypothesized to aid in cell attachment. The attachment study was repeated, with the addition of serum-free conditions. It was hypothesized that in the presence of serum, competitive binding was occurring with other proteins, and therefore the RGD peptide did not influence the attachment of ACLFs to the material. Again, scaffold discs were prepared, with and without the RGD peptide-polymer conjugate, and seeded with ACLFs either in complete or serum-free media. After a 4 h attachment period, all samples were covered with complete media for the remainder of the 24 h study. After 24 h, the WST-1 assay (Figure 21) was used to calculate cell number on the scaffolds (no peptide n=7, +RGD n=6).

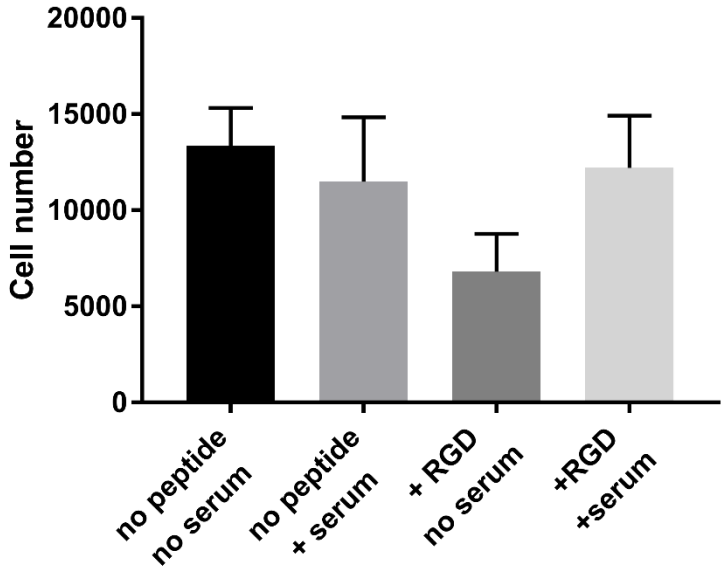

Figure 21 Comparison of cell number for scaffold discs made with and without peptide-polymer conjugate, in the presence of complete or serum-free media, calculated using WST-1 proliferation assay.

Again, there were no significant differences in attachment on the scaffolds made with the RGD peptide-polymer conjugate, regardless of whether serum was present or not. This result shows that, at the density of RGD used in the study, there was no influence on cell attachment even without competitive protein binding. For the serum-free conditions, the ACLFs were still able to attach to the scaffolds, even without RGD, without serum proteins adhered to the surface. This ability to attach can be explained by the secretion of fibronectin from the fibroblasts, as shown by Grinnell and Feld.[133] They demonstrated that human fibroblasts secreted fibronectin onto a surface within 10 minutes of seeding, promoting cellular attachment and spreading. This mechanism would explain the attachment of the ACLFs onto the scaffolds in the serum-free media in this study as well. The cell attachment studies demonstrated that the RGD peptide-polymer conjugate, at the concentration used in the study, had no significant effect on the attachment of ACLFs to the fibrous scaffolds. The lack of influence of the peptide ligand could be caused by a low density of RGD on the surface, and potentially at greater concentrations the peptide would influence cell attachment. Further, it has been shown that the spatial arrangement of RGD ligands is important in the formation of clusters and their effect on spreading and focal adhesions;[134–136] if RGD clustering is not occurring on the fibrous scaffolds, it could be responsible for the lack of improvement in fibroblast attachment. Further analysis, to determine the influence of the peptide on mechanotransduction and the resulting ECM composition, was performed.

5.3.2 Bioreactor Study

Rectangular 2.5 X 1.5 cm^2 fibre scaffolds, made with and without the RGD peptide-polymer conjugate, were prepared, sterilized, and seeded with ACLFs at a density of $3x10^4$ cells/cm^2. After 5 days, samples were rolled up and transferred either to the CellScale bioreactors for the dynamic conditions, or to new petri dishes for the static conditions. The scaffolds in the bioreactor were exposed to dynamic strain at 10%, 1 Hz, for 1 h each day. After 2 weeks, samples were removed from the bioreactors or dishes and digested in papain in preparation for analysis. Assays were performed to quantify the mass of dsDNA representative of total cell number (Figure 22), collagen (Figure 23), and sulfated GAG (Figure 24) in the scaffolds. Due to an issue with contamination early in the study, the n value for the samples without peptide is only 3, while the n values for the RGD samples are 7 (static) and 6 (dynamic).

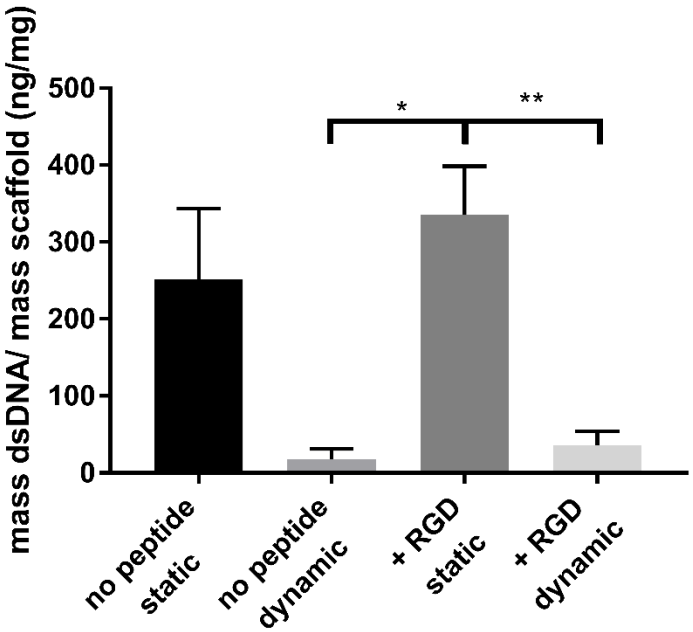

Figure 22: Mass of dsDNA per scaffold, normalized to scaffold weight. Comparing scaffolds with and without RGD peptide-polymer conjugate, and static vs. dynamic culture. ("*" = $p < 0.05$, "" = $p < 0.01$).**

Scaffolds made with the RGD peptide-polymer conjugate and cultured statically had significantly more dsDNA per scaffold at the end of the 2-week period than the dynamically cultured scaffolds made with or without RGD. It also appeared that, when comparing the scaffolds made without peptide, there was more dsDNA on scaffolds cultured statically than those cultured dynamically; however, these values were not statistically different. This result is consistent with previous work done by Surrao *et al.*[105]

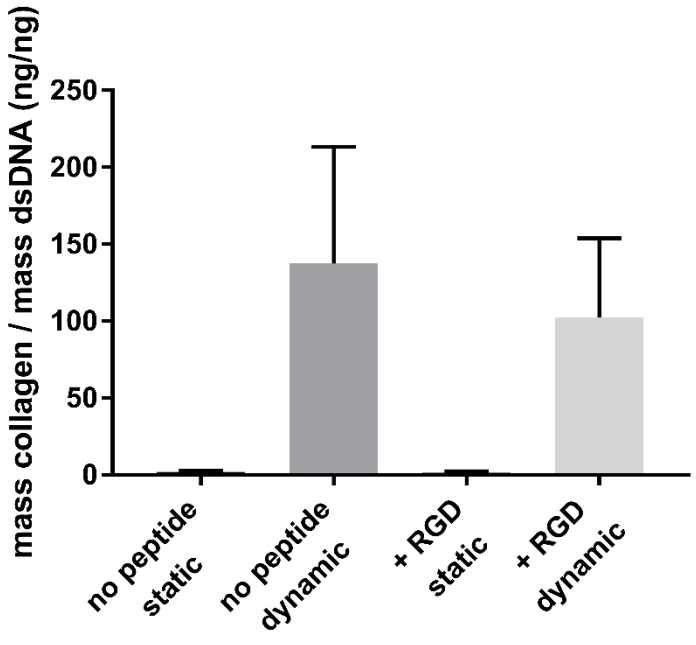

Figure 23: Mass of collagen per scaffold, normalized to mass of dsDNA. Comparing scaffolds with and without RGD peptide-polymer conjugate, and static vs. dynamic culture.

None of the conditions resulted in statistically different amounts of accumulated collagen within the scaffolds. However, the mean value for the amount of collagen per cell accumulated within the dynamically grown scaffolds was more than 50-fold greater than the mean value accumulated within the static scaffolds, for each of the respective systems.

This result indicates that the ACLFs produced more collagen in response to dynamic stimulation, than when cultured in static conditions, which is consistent with previous work[105], and could be promising for future bioreactor studies.

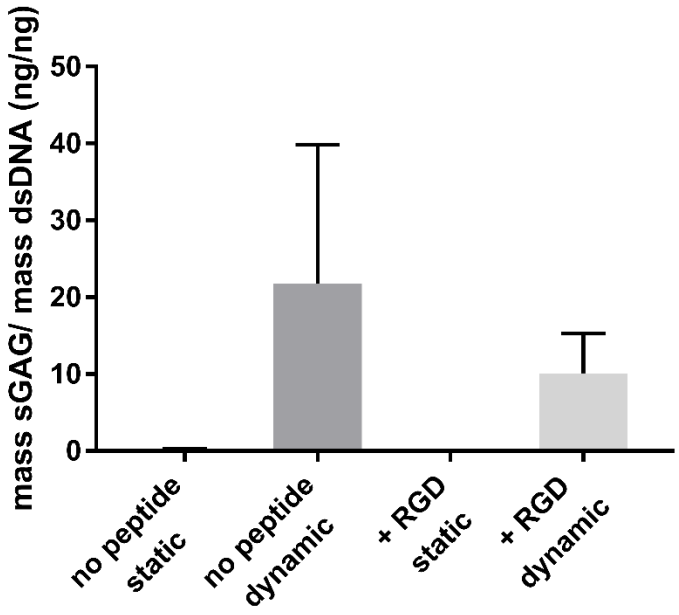

Figure 24: Mass of sulfated GAG per scaffold, normalized to mass of dsDNA. Comparing scaffolds with and without RGD peptide-polymer conjugate, and static vs. dynamic culture.

Again, there were no statistically significant differences between any of the conditions shown in Figure 24, when comparing GAG production per sample. Similar to the results shown with collagen production, the dynamically cultured scaffolds appear to produce more GAG than the statically cultured scaffolds, regardless of whether the peptide was present. While not statistically significant, the mean dynamic values were more than 100-fold greater than the mean static values. This trend could indicate that dynamically cultured cells produced more GAG in response to dynamic loading, when compared to static

conditions, which is again consistent with previous work[105] and promising for future bioreactor studies.

From the results of the assays, it is apparent that cell-seeded scaffolds cultured dynamically result in much lower DNA than those cultured statically, regardless of the addition of the RGD. It is hypothesized that the cells cultured dynamically directed more energy towards ECM production, and therefore had less energy to direct towards actively growing. Alternatively, the statically cultured cells were actively growing, and therefore directed less energy to ECM production. This explanation is corroborated by the results that show that the ACLFs cultured on dynamically stimulated scaffolds produced greater amounts of ECM than those cultured statically. This behaviour is well documented in the literature, and likely due to the fact that mechanical stretch increases the expression of integrin αV in ACLF cells.[109] The inclusion of the RGD peptide-polymer conjugate was not shown to influence ACLF behavior on the scaffolds; further analysis is necessary to determine ligand density and spacing, as RGD clustering may be necessary to improve focal adhesions and mechanotransduction, as described in the previous section.

Chapter 6

Conclusions

A bioinspired scaffold, electrospun from P(LLA-AC) and functionalized with the RGD motif, was successfully prepared. The RGD peptide was conjugated to a MAL-PEG-P(LLA-AC) copolymer via a Michael-type addition, which allowed for dissolution in the electrospinning solvent mixture. The resulting scaffold had an architecture and material properties comparable to the non-functionalized scaffold. Fibre diameter and scaffold porosity were compared using SEM imaging. The Young's modulus and toe regions of the constructs were measured using stress-strain curves obtained from uniaxial mechanical testing. Scaffolds were shown to withstand prolonged cyclic uniaxial strain in a bioreactor.

ACLFs were shown to attach to the scaffolds, whether or not the peptide-conjugate was included. Scaffolds, made with and without the peptide conjugate, were seeded with ACLFSs and cultured in bioreactors to determine the effect of dynamic loading on ECM production; the scaffolds were exposed to 10% strain at 1 Hz for an hour each day. Statically cultured scaffolds contained more dsDNA after 12 days than those cultured dynamically, regardless of the addition of the RGD peptide. Further, scaffolds cultured under dynamic stimulation produced greater quantities of collagen and GAG. No differences could be ascertained between the scaffolds made with or without the peptide-polymer conjugate.

6.1 Recommendations

An important step in the future of this project should be quantifying the amount of RGD peptide that is exposed to the seeded cells. While the mass of the peptide-polymer conjugate is known in relation to the bulk polymer for electrospinning, it would be beneficial to quantify the surface density of RGD on the final scaffolds. Surface quantification would allow for easier comparison with other studies, and for optimization of the peptide concentration, as well as in the consideration of RGD clustering. Chen *et al*. used X-ray photoelectron spectrometry to quantify the surface density of iodinated GRYDS peptide on their silk matrix;[78] a similar method could be considered.

The bioreactor study outlined in this thesis should be repeated with a greater n value. A better method to sterilize the scaffolds should be investigated, as there were issues with contamination that appeared to stem from the materials themselves. Modifications to the grips, or a method to sterilize parafilm, should be considered to protect the samples from the sharp edges of the metal grips in the bioreactor; if samples are not prematurely torn at the grips, there is a greater chance of retaining all seeded samples through the whole study. Additionally, the static scaffold samples should also be placed in a bioreactor with no dynamic programming, ensuring that they experience the same conditions as those cultured dynamically, and are effective controls. If greater n values can be obtained, the mechanical properties (Young's modulus and toe region) of the scaffolds should be measured to determine the effect of ECM accumulation.

To further investigate the effect of the RGD peptide, and any differences in surface modification, it would be beneficial to add additional negative controls to the study. Scaffolds could be electrospun with the bulk polymer as well as the MAL-PEG-P(LLA-AC) polymer (without the peptide), to determine if the PEG spacer influences the hydrophilicity of the material and the cellular response. Additionally, a scrambled peptide (using the same amino acids, but in a different order) could be used in the formulation to ensure that the cellular response is specific to the RGD integrin-binding sequence.

Further, bioreactor studies should be completed with ASCs as well as ACLFS. These should compare ASC:ACLF ratios of 1:0, 1:1 and 0:1, to investigate the effect of ASC co-culture on the quantity and composition of ECM production. Finally, the optimized scaffolds should be tested *in vivo*, using a rabbit model.

Bibliography

1. Chiu, S. S. The anterior tibial translocation. *Radiology* **239,** 914–915 (2006).
2. Murray, M. M. & Fleming, B. C. Biology of anterior cruciate ligament injury and repair: Kappa delta ann doner vaughn award paper 2013. *J. Orthop. Res.* **31,** 1501–1506 (2013).
3. Alentorn-Geli, E. *et al.* Prevention of non-contact anterior cruciate ligament injuries in soccer players. Part 1: Mechanisms of injury and underlying risk factors. *Knee Surgery, Sport. Traumatol. Arthrosc.* **17,** 705–729 (2009).
4. Krosshaug, T. *et al.* Mechanisms of anterior cruciate ligament injury in basketball: Video analysis of 39 cases. *Am. J. Sports Med.* **35,** 359–367 (2006).
5. Bahr, R. & Krosshaug, T. Understanding injury mechanisms: a key component of preventing injuries in sport. *Br. J. Sports Med.* **39,** 324–9 (2005).
6. Hewett, T. E., Myer, G. D. & Ford, K. R. Anterior cruciate ligament injuries in female athletes part 1, mechanisms and risk factors. *Am. J. Sports Med.* **34,** 299–311 (2006).
7. Ford, K. R. & Mclean, S. G. Biomechanical measures of neuromuscular control and valgus loading of the knee predict anterior cruciate ligament injury risk in female athletes a prospective study. *Am. J. Sports Med.* **33,** 492–501 (2005).
8. Noyes, F. R. *et al.* Arthroscopy in acute traumatic hemarthrosis of the knee. Incidence of anterior cruciate tears and other injuries. *J. Bone Joint Surg. Am.* **62,** 687–95, 757 (1980).
9. Liljedahl, S. O., Lindvall, N. & Wetterfors, J. Early diagnosis and treatment of acute ruptures of the anterior cruciate ligament; a clinical and arthrographic study of forty-eight cases. *J. Bone Joint Surg. Am.* **47,** 1503–1513 (1965).
10. Woo, S. L., Vogrin, T. M. & Abramowitch, S. D. Healing and repair of ligament injuries in the knee. *J. Am. Acad. Orthop. Surg.* **8,** 364–372 (2000).
11. Costa-Paz, M. *et al*. Spontaneous healing in complete ACL ruptures: A clinical and MRI study. *Clin. Orthop. Relat. Res.* **470,** 979–985 (2012).
12. Petrigliano, F. A., McAllister, D. R. & Wu, B. M. Tissue engineering for anterior cruciate ligament reconstruction: A review of current strategies. *Arthrosc. - J. Arthrosc. Relat. Surg.* **22,** 441–451 (2006).
13. Feagin, J. A. & Curl, W. W. Isolated tear of the anterior cruciate ligament: 5-year follow-up study. *Am. J. Sports Med.* **3,** 95–100 (1976).
14. Engebretsen, L. *et al*. A prospective, randomized study of three surgical techniques for treatment of acute ruptures of the anterior cruciate ligament. *Am. J. Sports Med.* **18,** 585–590 (1990).
15. Meunier, A., Odensten, M. & Good, L. Long-term results after primary repair or non-surgical treatment of anterior cruciate ligament rupture: A randomized study with a 15-year follow-up. *Scand. J. Med. Sci. Spor.* **17,** 230–237 (2007).
16. Vunjak-Novakovic, G. *et al*. Tissue engineering of ligaments. *Annu. Rev. Biomed. Eng.* **6,** 131–133 (2004).
17. Reinhardt, K. R., Hetsroni, I. & Marx, R. G. Graft selection for anterior cruciate ligament reconstruction: A level I systematic review comparing failure rates and functional outcomes. *Orthop. Clin. North Am.* **41,** 249–262 (2010).

18. Akoto, R. & Hoeher, J. Anterior cruciate ligament (ACL) reconstruction with quadriceps tendon autograft and press-fit fixation using an anteromedial portal technique. *BMC Musculoskelet. Disord.* **13,** 161 (2012).
19. Macaulay, A. A., Perfetti, D. C. & Levine, W. N. Anterior cruciate ligament graft choices. *Sports Health* **4,** 63–8 (2012).
20. Laurencin, C. T. & Freeman, J. W. Ligament tissue engineering: An evolutionary materials science approach. *Biomaterials* **26,** 7530–7536 (2005).
21. Garth, W. P. J. Current concepts regarding the anterior cruciate ligament. *Orthop. Rev.* **21,** 565–575 (1992).
22. Zoltan, D. J., Reinecke, C. & Indelicato, P. A. Synthetic and allograft anterior cruciate ligament reconstruction. *Clin. Sports Med.* **7,** 773–784 (1988).
23. Guidoin, M. F. *et al.* Analysis of retrieved polymer fiber based replacements for the ACL. *Biomaterials* **21,** 2461–74 (2000).
24. Hubbell, J. Biomaterials in tissue engineering. *Nat. Biotechnol.* (1995).
25. Rathbone, S., Maffulli, N. & Cartmell, S. H. Most British surgeons would consider using a tissue-engineered anterior cruciate ligament: A questionnaire study. *Stem Cells Int.* **2012,** (2012).
26. Strocchi, R. *et al.* The human anterior cruciate ligament: histological and ultrastructural observations. *J. Anat.* **180,** 515–519 (1992).
27. Duthon, V. B. *et al.* Anatomy of the anterior cruciate ligament. *Knee Surgery, Sport. Traumatol. Arthrosc.* **14,** 204–213 (2006).
28. Frank, C. *et al*. Normal ligament properties and ligament healing. *Clin. Orthop. Relat. Res.* **NA;,** 15–25 (1985).
29. Amiel, D. *et al*. Tendons and ligaments: A morphological and biochemical comparison. *J. Orthop. Res.* **1,** 257–265 (1983).
30. Chen, E. H. & Black, J. Materials design analysis of the prosthetic anterior cruciate ligament. *J. Biomed. Mater. Res.* **14,** 567–586 (1980).
31. Jones, R. S. *et al.* Mechanical properties of the human anterior cruciate ligament. *Clin Biomech* **10,** 339–344 (1995).
32. Woo, S. L.-Y. *et al*. Tensile properties of the human femur-anterior cruciate ligament-tibia complex. *Am. J. Sports Med.* **19,** 217–225 (1991).
33. Woo, S. L.-Y. *et al*. Biomechanics of knee ligaments: Injury, healing, and repair. *J. Biomech.* **39,** 1–20 (2006).
34. Dargel, J. *et al.* Biomechanics of the anterior cruciate ligament and implications for surgical reconstruction. *Strateg. Trauma Limb Reconstr.* **2,** 1–12 (2007).
35. Noyes, F. R. & Grood, E. S. The strength of the anterior cruciate ligament in humans and Rhesus monkeys. *J. Bone Joint Surg. Am.* **58,** 1074–82 (1976).
36. Gehlsen, K. *et al.* A synthetic peptide derived from the carboxyl terminus of the laminin a chain represents a binding site for the a3b1 integrin. *J. Cell Biol.* **117,** 449–459 (1992).
37. Wang, J. H.-C. C. Mechanobiology of tendon. *J. Biomech.* **39,** 1563–1582 (2006).
38. Murray, M. M. & Spector, M. Fibroblast distribution in the anteromedial bundle of the human anterior cruciate ligament: The presence of α-smooth muscle actin-positive cells. *J. Orthop. Res.* **17,** 18–27 (1999).
39. Van Eijk, F. *et al.* Tissue engineering of ligaments: a comparison of bone marrow stromal cells, anterior cruciate ligament, and skin fibroblasts as cell source. *Tissue*

Eng. **10,** 893–903 (2004).
40. Cooper, J. A. *et al.* Evaluation of the anterior cruciate ligament, medial collateral ligament, achilles tendon and patellar tendon as cell sources for tissue-engineered ligament. *Biomaterials* **27,** 2747–2754 (2006).
41. Dhinsa, B. S., Mahapatra, A. N. & Khan, W. S. Sources of adult mesenchymal stem cells for ligament and tendon tissue engineering. *Curr. Stem Cell Res. Ther.* **10,** 26–30 (2014).
42. Millard, S. M. & Fisk, N. M. Mesenchymal stem cells for systemic therapy: Shotgun approach or magic bullets? *BioEssays* **35,** 173–182 (2013).
43. Fennema, E. M. *et al*. The effect of bone marrow aspiration strategy on the yield and quality of human mesenchymal stem cells. *Acta orthopaedica* **80,** 618–21 (2009).
44. Gimble, J. M., Katz, A. J. & Bunnell, B. A. Adipose-derived stem cells for regenerative medicine. *Circulation Research* **100,** 1249–1260 (2007).
45. Kern, S. *et al*. Comparative analysis of mesenchymal stem cells from bone marrow, umbilical cord blood, or adipose tissue. *Stem cells* **24,** 1294–1301 (2006).
46. Izadpanah, R. *et al.* Biologic properties of mesenchymal stem cells derived from bone marrow and adipose tissue. *Journal of Cellular Biochemistry* **99,** 1285–1297 (2006).
47. Trumbull, A., Subramanian, G. & Yildirim-Ayan, E. Mechanoresponsive musculoskeletal tissue differentiation of adipose-derived stem cells. *Biomedical engineering online* **15,** 43 (2016).
48. Zhang, L. *et al.* Time-related changes in expression of collagen types I and III and of tenascin-C in rat bone mesenchymal stem cells under co-culture with ligament fibroblasts or uniaxial stretching. *Cell Tissue Res.* **332,** 101–109 (2008).
49. Fan, H. *et al*. Anterior cruciate ligament regeneration using mesenchymal stem cells and silk scaffold in large animal model. *Biomaterials* **30,** 4967–4977 (2009).
50. Ball, S. G., Shuttleworth, A. C. & Kielty, C. M. Direct cell contact influences bone marrow mesenchymal stem cell fate. *Int. J. Biochem. Cell Biol.* **36,** 714–727 (2004).
51. Schneider, P. R. A. *et al*. Three-dimensional high-density co-culture with primary tenocytes induces tenogenic differentiation in mesenchymal stem cells. *J. Orthop. Res.* **29,** 1351–1360 (2011).
52. Liu, X. *et al.* In vivo ectopic chondrogenesis of BMSCs directed by mature chondrocytes. *Biomaterials* **31,** 9406–9414 (2010).
53. Canseco, J. A. *et al.* Effect on ligament marker expression by direct-contact co-culture of mesenchymal stem cells and anterior cruciate ligament cells. *Tissue Eng. Part A* **18,** 2549–58 (2012).
54. Proffen, B. L. *et al*. Mesenchymal Stem Cells from the Retropatellar Fat Pad and Peripheral Blood Stimulate ACL Fibroblast Migration, Proliferation, and Collagen Gene Expression. *Connect. Tissue Res.* **54,** 1–8 (2012).
55. Cristino, S. *et al.* Analysis of mesenchymal stem cells grown on a three-dimensional HYAFF 11®-based prototype ligament scaffold. *J. Biomed. Mater. Res. A.* **73,** 275–283 (2005).
56. Altman, G. H. *et al.* Silk matrix for tissue engineered anterior cruciate ligaments. *Biomaterials* **23,** 4131–4141 (2002).

57. Li, X. & Snedeker, J. G. Wired silk architectures provide a biomimetic ACL tissue engineering scaffold. *J. Mech. Behav. Biomed. Mater.* **22,** 30–40 (2013).
58. Bellincampi, L. D. *et al*. Viability of fibroblast-seeded ligament analogs after autogenous implantation. *J. Orthop. Res.* **16,** 414–420 (1998).
59. Dunn, M. G. *et al*. Development of fibroblast-seeded ligament analogs for ACL reconstruction. *J. Biomed. Mater. Res.* **29,** 1363–1371 (1995).
60. Nöth, U. *et al.* Anterior cruciate ligament constructs fabricated from human mesenchymal stem cells in a collagen type I hydrogel. *Cytotherapy* **7,** 447–455 (2005).
61. Gentleman, E. *et al.* Mechanical characterization of collagen fibers and scaffolds for tissue engineering. *Biomaterials* **24,** 3805–3813 (2003).
62. Chvapil, M. *et al*. Collagen fibers as a temporary scaffold for replacement of ACL in goats. *J. Biomed. Mater. Res.* **27,** 313–325 (1993).
63. Tovar, N. *et al.* A comparison of degradable synthetic polymer fibers for anterior cruciate ligament reconstruction. *J. Biomed. Mater. Res. A.* **93,** 738–747 (2010).
64. Dürselen, L. *et al.* Control of material stiffness during degradation for constructs made of absorbable polymer fibers. *J. Biomed. Mater. Res. B.* **67,** 697–701 (2003).
65. Sahoo, S. *et al*. Characterization of a novel polymeric scaffold for potential application in tendon/ligament tissue engineering. *Tissue Eng.* **12,** 91–99 (2006).
66. Viidik A. in *Extracellular matrix, 1, Tissue Function* (eds. Lanza, R., Langer, R. & Chick, W.) 303—27 (RG Landes and Academic Press, 1996).
67. Kew, S. J. *et al.* Regeneration and repair of tendon and ligament tissue using collagen fibre biomaterials. *Acta Biomater.* **7,** 3237–3247 (2011).
68. Parenteau-Bareil, R., Gauvin, R. & Berthod, F. Collagen-based biomaterials for tissue engineering applications. *Materials* **3,** 1863–1887 (2010).
69. Cornwell, K. G. *et al*. Crosslinking of discrete self-assembled collagen threads: Effects on mechanical strength and cell-matrix interactions. *J. Biomed. Mater. Res. A.* **80,** 362–371 (2007).
70. Weadock, K. S. *et al*. Physical crosslinking of collagen fibers: Comparison of ultraviolet irradiation and dehydrothermal treatment. *J. Biomed. Mater. Res.* **29,** 1373–1379 (1995).
71. Wiig, M. E. *et al.* The early effect of high molecular weight hyaluronan (hyaluronic acid) on anterior cruciate ligament healing: An experimental study in rabbits. *J. Orthop. Res.* **8,** 425–434 (1990).
72. Shao, H.-J. *et al*. The phenotypic responses of human anterior cruciate ligament cells cultured on poly(epsilon-caprolactone) and chitosan. *J. Biomed. Mater. Res. A.* **93,** 1297–1305 (2010).
73. Deepthi, S. *et al*. Chitosan-hyaluronic acid hydrogel coated poly(caprolactone) multiscale bilayer scaffold for ligament regeneration. *Chem. Eng. J.* **260,** 478–485 (2015).
74. Sarukawa, J. *et al.* Effects of chitosan-coated fibers as a scaffold for three-dimensional cultures of rabbit fibroblasts for ligament tissue engineering. *J. Biomater. Sci. Polym. Ed.* **22,** 717–732 (2011).
75. Hayami, J. Development of a Biomimetic Scaffold for Ligament Tissue Engineering. (2006). Queen's University, M.Asc. dissertation.
76. Altman, G. H. *et al.* Silk-based biomaterials. *Biomaterials* **24,** 401–416 (2003).

77. Vepari, C. & Kaplan, D. L. Silk as a biomaterial. *Prog. Polym. Sci.* **32,** 991–1007 (2007).
78. Chen, J. *et al.* Human bone marrow stromal cell and ligament fibroblast responses on RGD-modified silk fibers. *J. Biomed. Mater. Res. A.* **67,** 559–570 (2003).
79. Wohlrab, S. *et al.* Cell adhesion and proliferation on RGD-modified recombinant spider silk proteins. *Biomaterials* **33,** 6650–6659 (2012).
80. Chen, X. *et al.* Ligament regeneration using a knitted silk scaffold combined with collagen matrix. *Biomaterials* **29,** 3683–3692 (2008).
81. Middleton, J. C. & Tipton, A. J. Synthetic biodegradable polymers as orthopedic devices. *Biomaterials* **21,** 2335–2346 (2000).
82. Pitt, G. G., *et al*. Aliphatic polyesters II. The degradation of poly (DL-lactide), poly (E-caprolactone), and their copolymers in vivo. *Biomaterials* **2,** 215–220 (1981).
83. Pitt, C. G. *et al*. Aliphatic polyesters. I. The degradation of poly(E-caprolactone) in vivo. *J. Appl. Polym. Sci.* **26,** 3779–3787 (1981).
84. Vacanti, N. M. *et al.* Localized delivery of dexamethasone from electrospun fibers reduces the foreign body response. *Biomacromolecules* **13,** 3031–3038 (2012).
85. Prime, E. L. *et al*. Addition of biological functionality to poly(ε-caprolactone) films. *Biomacromolecules* **8,** 2416–2421 (2007).
86. Ilagan, B. G. & Amsden, B. G. Surface modifications of photocrosslinked biodegradable elastomers and their influence on smooth muscle cell adhesion and proliferation. *Acta Biomater.* **5,** 2429–2440 (2009).
87. Santiago, L. Y. *et al*. Peptide-surface modification of poly(caprolactone) with laminin-derived sequences for adipose-derived stem cell applications. *Biomaterials* **27,** 2962–2969 (2006).
88. Lu, H. H. *et al.* Anterior cruciate ligament regeneration using braided biodegradable scaffolds: In vitro optimization studies. *Biomaterials* **26,** 4805–4816 (2005).
89. Surrao, D. C., Waldman, S. D. & Amsden, B. G. Biomimetic poly(lactide) based fibrous scaffolds for ligament tissue engineering. *Acta Biomater.* **8,** 3997–4006 (2012).
90. Chen, F., Hayami, J. W. S. & Amsden, B. G. Electrospun poly(l -lactide-co - acryloyl carbonate) fiber scaffolds with a mechanically stable crimp structure for ligament tissue engineering. *Biomacromolecules* **15,** 1593–1601 (2014).
91. Cooper, J. a *et al.* Biomimetic tissue-engineered anterior cruciate ligament replacement. *Proc. Natl. Acad. Sci. U. S. A.* **104,** 3049–3054 (2007).
92. Frank, C. *et al.* Medial collateral ligament healing. A multidisciplinary assessment in rabbits. *Am. J. Sports Med.* **11,** 379–89 (1983).
93. Zhu, B. *et al*. Alignment of osteoblast-like cells and cell-produced collagen matrix induced by nanogrooves. *Tissue Eng.* **11,** 825–834 (2005).
94. Teixeira, A. I. *et al*. Epithelial contact guidance on well-defined micro- and nanostructured substrates. *J. Cell Sci.* **116,** 1881–92 (2003).
95. Walboomers, X. F. *et al*. Contact guidance of rat fibroblasts on various implant materials. *J. Biomed. Mater. Res.* **47,** 204–212 (1999).
96. Freeman, J. W., Woods, M. D. & Laurencin, C. T. Tissue engineering of the anterior cruciate ligament using a braid-twist scaffold design. *J. Biomech.* **40,**

2029–2036 (2007).
97. Freeman, J. W. *et al.* Evaluation of a hydrogel-fiber composite for ACL tissue engineering. *J. Biomech.* **44,** 694–699 (2011).
98. Dunn, M. G. *et al*. Preliminary development of a collagen-PLA composite for ACL reconstruction. *J. Appl. Polym. Sci.* **63,** 1423–1428 (1995).
99. Gentleman, E. *et al*. A. Development of ligament-like structural organization and properties in cell-seeded collagen scaffolds in vitro. *Ann. Biomed. Eng.* **34,** 726–736 (2006).
100. Lukáš, D. *et al.* Physical principles of electrospinning (Electrospinning as a nano-scale technology of the twenty-first century). *Text. Prog.* **41,** 59–140 (2009).
101. Petrigliano, F. A. *et al.* In Vivo Evaluation of Electrospun Polycaprolactone Graft for Anterior Cruciate Ligament Engineering. *Tissue Eng. Part A* **21,** 150127064142004 (2014).
102. Thayer, P. S. *et al.* Cellularized cylindrical fiber/hydrogel composites for ligament tissue engineering. *Biomacromolecules* **15,** 75–83 (2014).
103. Vaquette, C. *et al.* Aligned poly(L-lactic-co-ε-caprolactone) electrospun microfibers and knitted structure: A novel composite scaffold for ligament tissue engineering. *J. Biomed. Mater. Res. A.* **94,** 1270–1282 (2010).
104. Surrao, D. C. *et al*. Self-crimping, biodegradable, electrospun polymer microfibers. *Biomacromolecules* **11,** 3624–3629 (2010).
105. Surrao, D. C. *et al*. A crimp-like microarchitecture improves tissue production in fibrous ligament scaffolds in response to mechanical stimuli. *Acta Biomater.* **8,** 3704–3713 (2012).
106. Spalazzi, J. P. *et al*. Development of controlled matrix heterogeneity on a triphasic scaffold for orthopedic interface tissue engineering. *Tissue Eng.* **12,** 3497–3508 (2006).
107. Spalazzi, J. P. *et al.* In vivo evaluation of a multiphased scaffold designed for orthopaedic interface tissue engineering and soft tissue-to-bone integration. *J. Biomed. Mater. Res. A.* **86,** 1–12 (2008).
108. He, P. *et al*. In vitro ligament–bone interface regeneration using a trilineage coculture system on a hybrid silk scaffold. *Biomacromolecules* **13,** (2012).
109. Tetsunaga, T. *et al.* Mechanical stretch stimulates integrin αVβ3-mediated collagen expression in human anterior cruciate ligament cells. *J. Biomech.* **42,** 2097–2103 (2009).
110. Kreja, L. *et al.* Effects of mechanical strain on human mesenchymal stem cells and ligament fibroblasts in a textured poly(l-lactide) scaffold for ligament tissue engineering. *J. Mater. Sci. Mater. Med.* **23,** 2575–2582 (2012).
111. Altman, G. H. *et al.* Cell differentiation by mechanical stress. *FASEB J.* **16,** 270–272 (2002).
112. Kaneko, D. *et al.* Temporal effects of cyclic stretching on distribution and gene expression of integrin and cytoskeleton by ligament fibroblasts in vitro. *Connect. Tissue Res.* **50,** 263–269 (2009).
113. Hannafin, J. A. *et al*. Effect of cyclic strain and plating matrix on cell proliferation and integrin expression by ligament fibroblasts. *J. Orthop. Res.* **24,** 149–158 (2006).
114. Henshaw, D. R. *et al*. A. Canine ACL fibroblast integrin expression and cell

alignment in response to cyclic tensile strain in three-dimensional collagen gels. *J. Orthop. Res.* **24,** 481–490 (2006).
115. Ma, J. *et al*. Cyclic stretch induced gene expression of extracellular matrix and adhesion molecules in human periodontal ligament cells. *Arch. Oral Biol.* **60,** 447–455 (2015).
116. Chiquet, M. *et al*. From mechanotransduction to extracellular matrix gene expression in fibroblasts. *Biochim. Biophys. Acta - Mol. Cell Res.* **1793,** 911–920 (2009).
117. Ide, A. *et al.* Collagen hybridization with poly(L-lactic acid) braid promotes ligament cell migration. *Mater. Sci. Eng. C* **17,** 95–99 (2001).
118. Funakoshi, T. *et al.* Novel chitosan-based hyaluronan hybrid polymer fibers as a scaffold in ligament tissue engineering. *J. Biomed. Mater. Res. A.* **74,** 338–346 (2005).
119. Majima, T. *et al.* Chitosan-based hyaluronan hybrid polymer fibre scaffold for ligament and tendon tissue engineering. *Proc. Inst. Mech. Eng. H.* **221,** 537–546 (2007).
120. Rustad, K. C., Wong, V. W. & Gurtner, G. C. The role of focal adhesion complexes in fibroblast mechanotransduction during scar formation. *Differentiation* **86,** 87–91 (2013).
121. Schreck, P. J. *et al*. Integrin display increases in the wounded rabbit medial collateral ligament but not the wounded anterior cruciate ligament. *J. Orthop. Res.* **13,** 174–183 (1995).
122. Bhargava, M. M. *et al.* Differential expression of integrin subunits in canine knee ligament fibroblasts. *J. Orthop. Res.* **17,** 748–754 (1999).
123. Plow, E. F. *et al*. Ligand binding to integrins. *J. Biol. Chem.* **275,** 21785–21788 (2000).
124. Frith, J. E. *et al*. Tailored integrin–extracellular matrix interactions to direct human mesenchymal stem cell differentiation. *Stem Cells and Development* **21,** 2442–2456 (2012).
125. Wang, P.-Y. *et al.* Modulation of cell attachment and collagen production of anterior cruciate ligament cells via submicron grooves/ridges structures with different cell affinity. *Biotechnol. Bioeng.* **110,** 327–37 (2013).
126. Chao, P. G. *et al.* Electrospun microcrimped fibers with nonlinear mechanical properties enhance ligament fibroblast phenotype. *Biofabrication* **6,** 35008 (2014).
127. Nair, D. P. *et al.* The thiol-Michael addition click reaction: A powerful and widely used tool in materials chemistry. *Chem. Mater.* **26,** 724–744 (2014).
128. Chen, W. *et al.* Versatile synthesis of functional biodegradable polymers by combining ring-opening polymerization and postpolymerization modification via michael-type addition reaction. *Macromolecules* **43,** 201–207 (2010).
129. Farah, S., Anderson, D. & Langer, R. Physical and mechanical properties of PLA, and their functions in widespread applications—a comprehensive review. *Adv. Drug Deliv. Rev.* **107,** 367 (2016).
130. Russo, J. *et al.* in *Techniques and Methodological Approaches in Breast Cancer Research* 75–102 (2014). doi:10.1007/978-1-4939-0718-2_3
131. Isidro-Llobet, A., Alvarez, M. & Albericio, F. Amino acid-protecting groups. *Chem. Rev.* **109,** 2455–2504 (2009).

132. Skelley, N. W. *et al.* Differences in the microstructural properties of the anteromedial and posterolateral bundles of the anterior cruciate ligament. *Am. J. Sports Med.* **43,** 928–36 (2015).
133. Grinnell, F. & Feld, M. K. Initial adhesion of human fibroblasts in serum-free medium: Possible role of secreted fibronectin. *Cell* **17,** 117–129 (1979).
134. Maheshwari, G. *et al*. Cell adhesion and motility depend on nanoscale RGD clustering. *J. Cell Sci.* **113,** 1677–1686 (2000).
135. Cavalcanti-Adam, E. A. *et al.* Lateral spacing of integrin ligands influences cell spreading and focal adhesion assembly. *Eur. J. Cell Biol.* **85,** 219–224 (2006).
136. Massia, S. P. & Hubbell, J. A. An RGD spacing of 440 nm is sufficient for fibroblast spreading and 140nm for focal contact and stress fiber formation. *J. Cell Biol.* **114,** 1089–1100 (1991).